NONLINEAR INTERACTIONS AMONG STANDING SURFACE AND INTERNAL GRAVITY WAVES

by

Terrence Michael Joyce

B.S., Rose Polytechnic Institute

(1968)

SUBMITTED IN PARTIAL FULFILLMENT OF THE
REQUIREMENTS FOR THE DEGREE OF
DOCTOR OF SCIENCE

at the

MASSACHUSETTS INSTITUTE OF TECHNOLOGY

and the

WOODS HOLE OCEANOGRAPHIC INSTITUTION

June, 1972

Signature of Author.....
Joint Program in Oceanography, Massachusetts Institute of Technology - Woods Hole Oceanographic Institution, and Department of Earth and Planetary Sciences, and Department of Meteorology, Massachusetts Institute of Technology, June 1972

Certified by.....
Thesis Supervisor

Accepted by.....
Chairman, Joint Oceanography Committee in the Earth Sciences, Massachusetts Institute of Technology - Woods Hole Oceanographic Institution

NONLINEAR INTERACTIONS AMONG STANDING SURFACE AND INTERNAL GRAVITY WAVES

by
Terrence Michael Joyce

Submitted to the Department of Meteorology on 5 May 1972
in Partial Fulfillment of the Requirements for
the Degree of Doctor of Science.

ABSTRACT

A laboratory study has been undertaken to measure the momentum transfer from surface to internal gravity waves in a nonlinear, resonant interaction. The interacting waves form triads for which $\sigma_{1s} - \sigma_{2s} \pm \sigma_I = 0$ and $\kappa_{1s} - \kappa_{2s} \pm \kappa_I = 0$; σ_j and κ_j being the frequency and wavenumber of the jth wave. In particular, the experiment is designed to model a generating mechanism for high frequency, oceanic internal waves. Unlike previously published results involving single triplets of interacting waves, all waves here considered are standing waves. The growth to steady state of a resonant internal wave is observed while two deep water surface eigen modes are simultaneously forced by a paddle. Results are compared to theoretical predictions which assume, ab initio, all waves to be standing. Inclusion of viscous side wall dissipation and slight detuning permit predictions of steady state amplitudes and phases as well as initial growth rates. Good agreement is found between predicted and measured amplitudes and phases. The experiments also suggest that the internal wave in a resonant triad can act as a catalyst, permitting appreciable energy transfer among surface waves.

Thesis Supervisor: Robert C. Beardsley
Title: Associate Professor of Oceanography

ACKNOWLEDGEMENTS

The author wishes to thank E. Bean and J. Mazzarini for their advice and labor during the construction of nearly all the mechanical apparatus, and K. Morey for his help with the electronics. Professor Eric Mollo-Christensen made several important contributions to experimental techniques and data handling. For the preparation of this manuscript, the author is indebted to W. Simmons for his comments, Kate Higgins and Barbara Wysochansky for the typing, V. Livada for the figures, and S. Bernbaum for the photographs. Above all others, the author thanks his wife, Karen, and his thesis advisor, Robert Beardsley, who made this work both enjoyable and possible.

TABLE OF CONTENTS

PLATES PAGE

LIST OF FIGURES PAGE

LIST OF FIGURES CONTINUED PAGE

CHAPTER I. Introduction

In the past twelve years, resonant wave-wave interactions in fluid mechanics have been studied a great deal. The original suggestion by Phillips (1960) that irrotational surface gravity waves would exhibit such an interaction was the first in a series of papers on resonantly interacting surface gravity waves to emerge over a period of three years.* An experiment was suggested by Longuet-Higgins (1962) to test the predictions made and two experiments were reported four years later which displayed many of the characteristics of the theory. The experiments were performed by Longuet-Higgins and Smith (1966) and McGoldrick, Phillips, Huang and Hodgson (1966). The interaction among deep water surface gravity waves was shown to occur at third order in the wave slope or Stokes ordering parameter $\epsilon = \chi a$, where $\chi = 2\pi$(wavelength)$^{-1}$ and a is the amplitude of the same wave. As predicted, the interaction was weak and great care needed to be taken in the experiments. While these experiments were being conducted, other types of waves were considered which could interact at second order in ϵ. McGoldrick (1965) suggested that capillary gravity waves could interact at this order. Ball (1964) and Thorpe (1966 A,B) presented theoretical evidence for the interaction between surface and internal progressive gravity waves, and among internal gravity waves. Hasselmann (1966) presented a general theory for geophysical nonlinear interactions drawing an analogy with quantum field scattering theory. Experiments have

*See for example Proc. Roy. Soc. A, 299 (1967) for a review of the state of art up to 1966.

recently been reported by McGoldrick (1970) and Kim and Hanratty (1971) for progressive capillary-gravity waves, and by Martin, Simmons and Wunsch (1969) for progressive internal waves. Thorpe (1966A) suggested an experiment in which two progressive surface gravity waves could be made to resonantly generate an internal wave. The experiment, however, was never done. In all of the above work (except for capillary-gravity waves), at least three waves are necessary to form a triad. For surface gravity waves, interactions among four waves are also possible.

It was soon realized that these theories for triad or quartet resonances could also explain the instability of a finite amplitude progressive wave. Benjamin and Feir (1967) and Phillips (1967) used these arguments to explain the ultimate breakup of a nonlinear, progressive Stokes wave due to side band resonances. Davis and Acrivos (1967) used a resonant interaction approach to explain the observed breakdown of a progressive internal wave in a diffuse, two-layer density field. Hasselmann (1967) has presented a general criterion for nonlinear wave stability. The predictions of this theory were verified by McEwan (1971) in an experiment dealing with the finite amplitude instability of standing internal waves in a linear stratification. Martin, Simmons and Wunsch (1972) have reported similar instabilities for progressive internal gravity waves. Resonant nonlinear instability has been suggested by Craik (1971) as an important mechanism in the turbulent breakdown of a laminar boundary layer. Clearly the importance of the resonant wave interaction mechanism has not yet been fully realized. It provides an avenue for the exchange of mechanical energy among different

frequencies and scales of motion in geophysical fluids.

One possible application of this mechanism is that of the generation of oceanic internal waves by high frequency surface waves. Kenyon (1968) considered this interaction and concluded that over much of the ocean it was less important than interactions among surface or internal waves separately. For his oceanic model, he chose a constant Brunt-Vaisälä frequency stratification. It will be shown in what follows that the surface-internal wave interaction can be important over much of the ocean if a near surface thermocline is present.

An experiment has been conducted in which two high frequency surface waves are generated by a wavemaker and a resonant internal wave is observed to grow. Both a constant Brunt-Väisälä and diffuse two-layer stratification are considered in detail. Unlike previous work, the experiments described here utilize three resonant standing waves in which two are externally produced. A theoretical approach is also taken which assumes ab initio all waves to be standing. The advantage of this approach to the study of the interaction of surface and internal gravity waves lies in the simplicity of the experiment. To be more precise, the resonant growth of an internal wave can be observed as a function of time in a relatively small wave tank instead of the growth of the resonant wave with distance in a large wave tank.

In the following chapter the experiment will be described. Chapters III and IV will present the theory for the two layer and linear stratifications, respectively. In Chapter V these predictions will be compared to experimental data. A discussion of the results constitutes the

final section of that chapter. In addition, two short appendices, experimental and theoretical, contain calibrations and equations not essential to the main thrust of this work.

CHAPTER II. Description of the Experiment

A. Apparatus

The experimental work was conducted in a wave tank especially built for this study. It was constructed with plate glass sides, plexiglass bottom and ends, and a steel frame supporting structure. The tank was 2.0 meters long, 0.2 meters wide and 1.0 meter deep. Two plexiglass end inserts enabled the working length of the tank to be adjusted. For most of the experiments, the length was kept at 1.8 meters.

The wave tank was filled from two 55 gallon polyethylene barrels which were supported directly above the wave tank, thus minimizing floor space requirements. A basic state of linear density stratification was easily formed using a method used successfully by Cacchione (1970). Two reservoirs, one filled with fresh water, the other salt water, were connected via a siphon. As fresh water flowed down into the wave tank, salt water was introduced and mixed into the fresh water reservoir. Figure II-1 schematically shows the filling apparatus. Figure II-2 shows the actual variation of density with depth over a period of a few days. An American Optical refractometer (model 10402) was used to measure the index of refraction of a milliliter sample to one part in 10^5. Calibration permitted density to be determined to five parts in 10^5. The calibrating procedure and results can be found in the experimental appendix. Fluid samples were withdrawn from the tank at selected depths by a one meter long hypodermic needle and syringe.

Surface waves were generated with a plunger-type paddle in the shape of a 30°-60°-90° wedge (with forcing surface being inclined 30° from the vertical). In order to reduce mechanical vibration, the wave

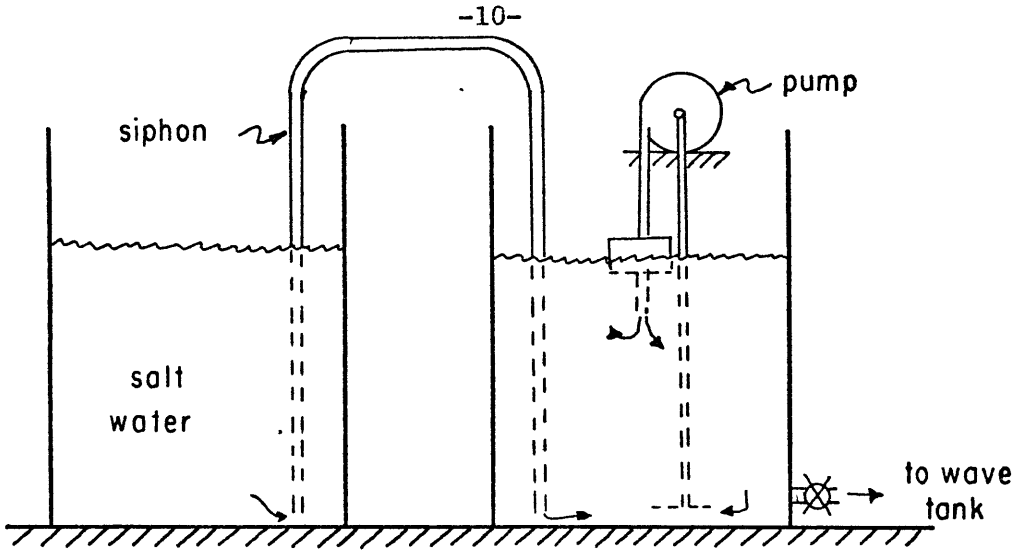

Figure II-1 Filling Apparatus

Figure II-2 $\rho(z)$ versus depth over 3-day interval

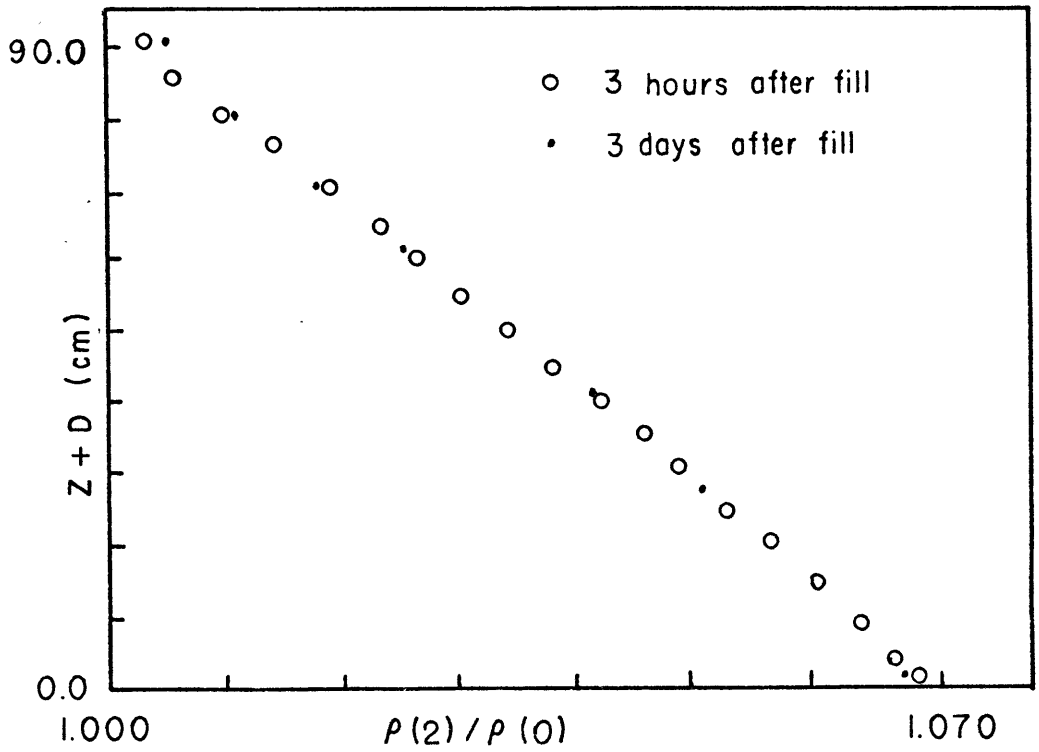

maker was supported independently of the wave tank structure. Even so, mechanical vibration due to the rubbing of the paddle against the tank was a source of noise. The paddle was driven vertically by two synchronous motors, two eccentric drives, and a mechanical adder. Eccentric driving produced higher harmonics in the vertical excursions of each shaft before addition. Shaft harmonics were less than 3% of the fundamental frequency. The motion of the paddle was then a sum of the motion of the two eccentric shafts. Plate II-1 shows the wavemaker. A differential gear and a resolver are also discernible between the two drive shafts. The electrical output of the resolver was approximately a sinusoidal function of time with a frequency equal to the difference frequency of the two motors. Each synchronous motor had an internal gear reduction of sixteen and was driven by a stable audio oscillator and a fifty watt DC through audio power amplifier. Continuous change of frequency of both motors was thus possible with this arrangement. One audio oscillator was a Hewlett-Packard (model 204C) with a rated stability of .05%. The second frequency source was a General Radio digital frequency synthesizer (model 1161-A) with a stability of .01%. Net motion of the paddle was measured by a simple rack and potentiometer arrangement.

Surface wave amplitude was detected by a transistorized wave gauge described in detail by McGoldrick (1969). The probe itself was of the capacitance type: a replaceable piece of coated magnet wire 0.04" in diameter. The amplitude and phase response of the circuitry was flat over a range of frequencies 0-10hz. Characteristics were not tested

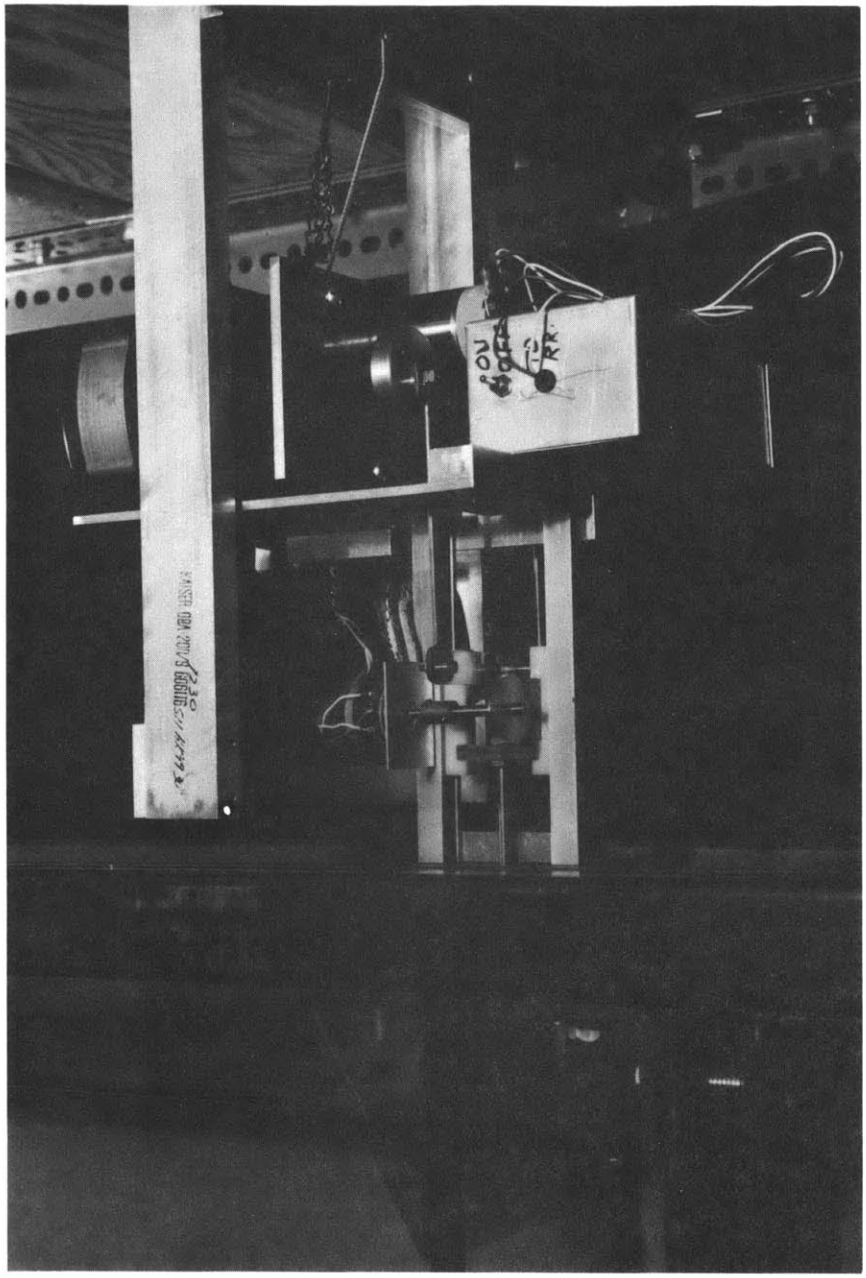

Plate II- Wavemaker

beyond 10 hz. Amplitude resolution of the whole device was limited by the ability of the experimenter to keep the fluid surface free from contaminants. A surface active agent such as Alcinox was used to reduce the surface tension at the air-"scum" interface. A sheet of saran wrap was always kept over the top of the wave tank. This helped keep the surface clean and the evaporative losses to a millimeter thick layer of water per day. With the wave gauge, resolution of 0.05 mm was possible. Further details of this instrument as well as other pertinent experimental information to what follows can be found in the experimental appendix.

The presence of internal oscillations was detected in two ways. A Sanborn differential pressure transducer (model 268B) was used in the absolute mode to measure departures of pressure from local mean values at selected points in the fluid. The mounting and use of this probe is shown in plate II-2. The transducer proved to be a versatile and reliable instrument for both linear and diffuse two-layer stratifications alike. Fluctuations of 0.02 mm H_2O were measurable. Beardsley (1970) obtained a resolution of 5×10^{-3} mm H_2O by cross correlating the pressure signal with a reference sinusoid of the same frequency. Depending on the density structure, a pressure resolution of .02 mm H_2O corresponded typically to a vertical particle excursion of 0.3 mm. Surface wave influence was kept to a minimum by keeping the pressure probe at least one surface wavelength (20 cm) below the free surface. In addition to internal measurements, neutrally buoyant particles made to the desired density were placed in the fluid. The particles were made by mixing together carbon tetrachloride and heptane. Diphenylthiocarba-

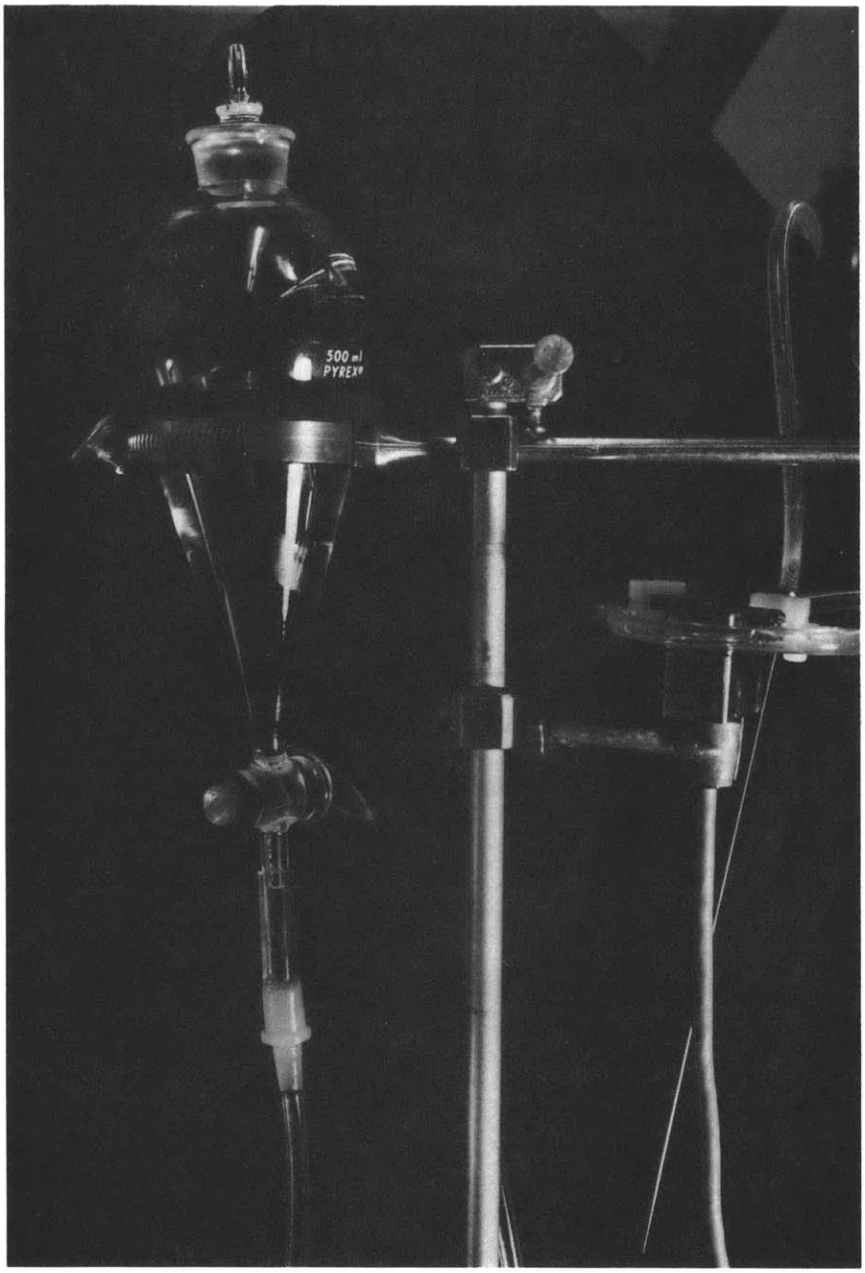

Plate II-2 Flushing reservoir and pressure transducer

zone, an intense green dye, soluble in CCl_4, increased the contrast between the particles and the background. Potassium permangenate crystals dropped into the tank during an experiment provided a visualization of the horizontal velocity field. For linear stratifications, horizontal lines of a highly nondiffusive dye (Blue Dextran 2000) were inserted during the filling process. These lines complimented the permangenate streaks by giving the field of vertical velocity. Back lighting through a diffuser enabled 16 mm moving pictures to be taken. The quantitative data for the internal oscillations, however, came from the pressure transducer and the particle amplitudes. Figure II-3 shows schematically the physical location of some of the apparatus.

B. Procedure

The procedure varied with the type of experiment being done, but several steps were common to all experiments. Before stratifying the wave tank, the fluids were allowed to outgas and come to thermal equilibrium with room temperature. Ordinarily one or two days was allowed for this step. After the tank was filled, both movable ends were gently placed in position, and the surface wave paddle was inserted to its fixed equilibrium depth. The surface eigen modes were then determined by sweeping one of the motors through a range of frequencies while observing on an oscilliscope the output of a wave gauge placed at the end opposite the wavemaker. Response curves obtained were then used to select surface eigen frequencies. A typical response curve is shown in figure II-4. Prior calculation had insured that, for the proper choices of length and depth of tank and the stratification, an internal eigen

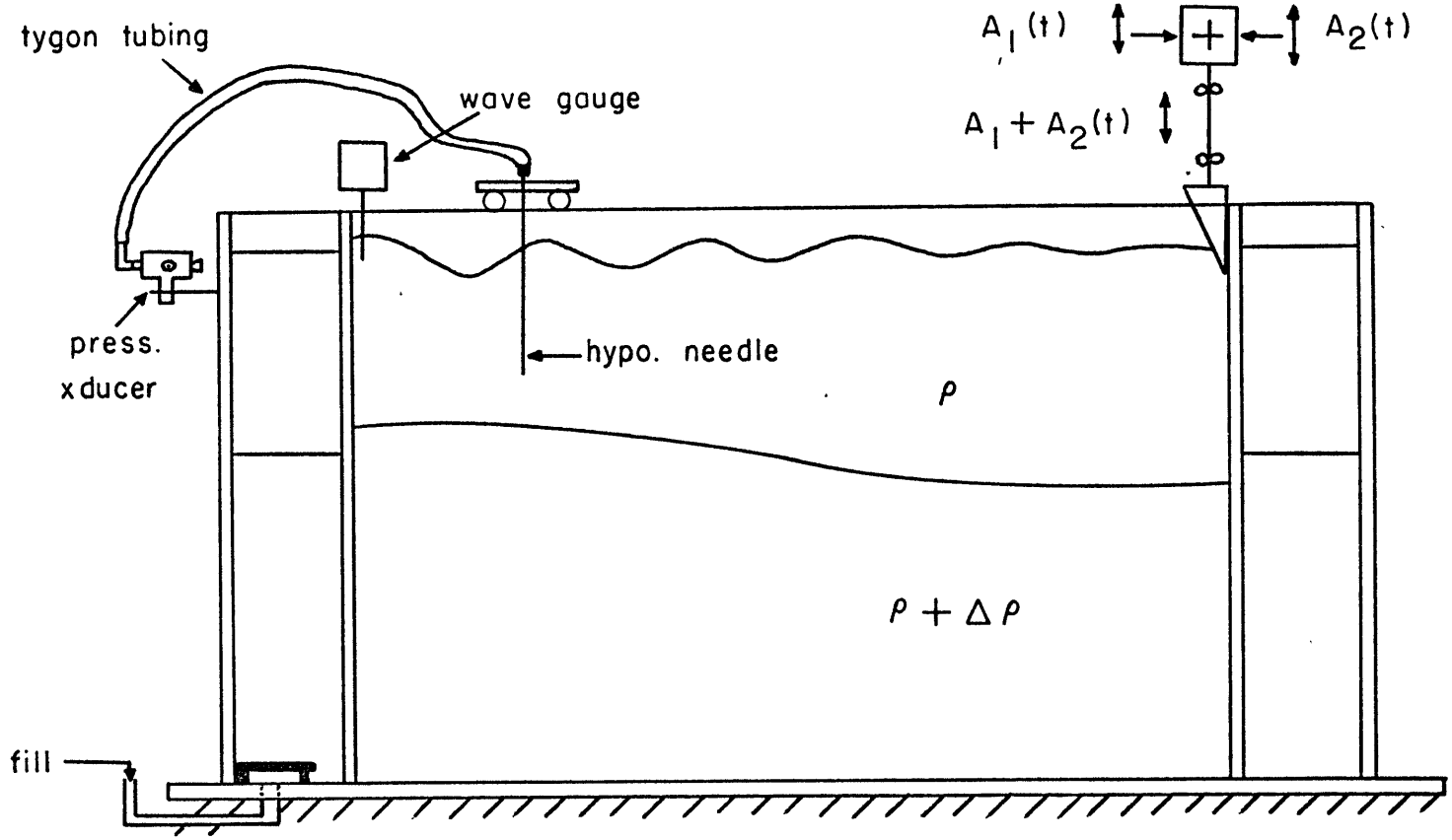

Figure II-3 Schematic of mechanical apparatus

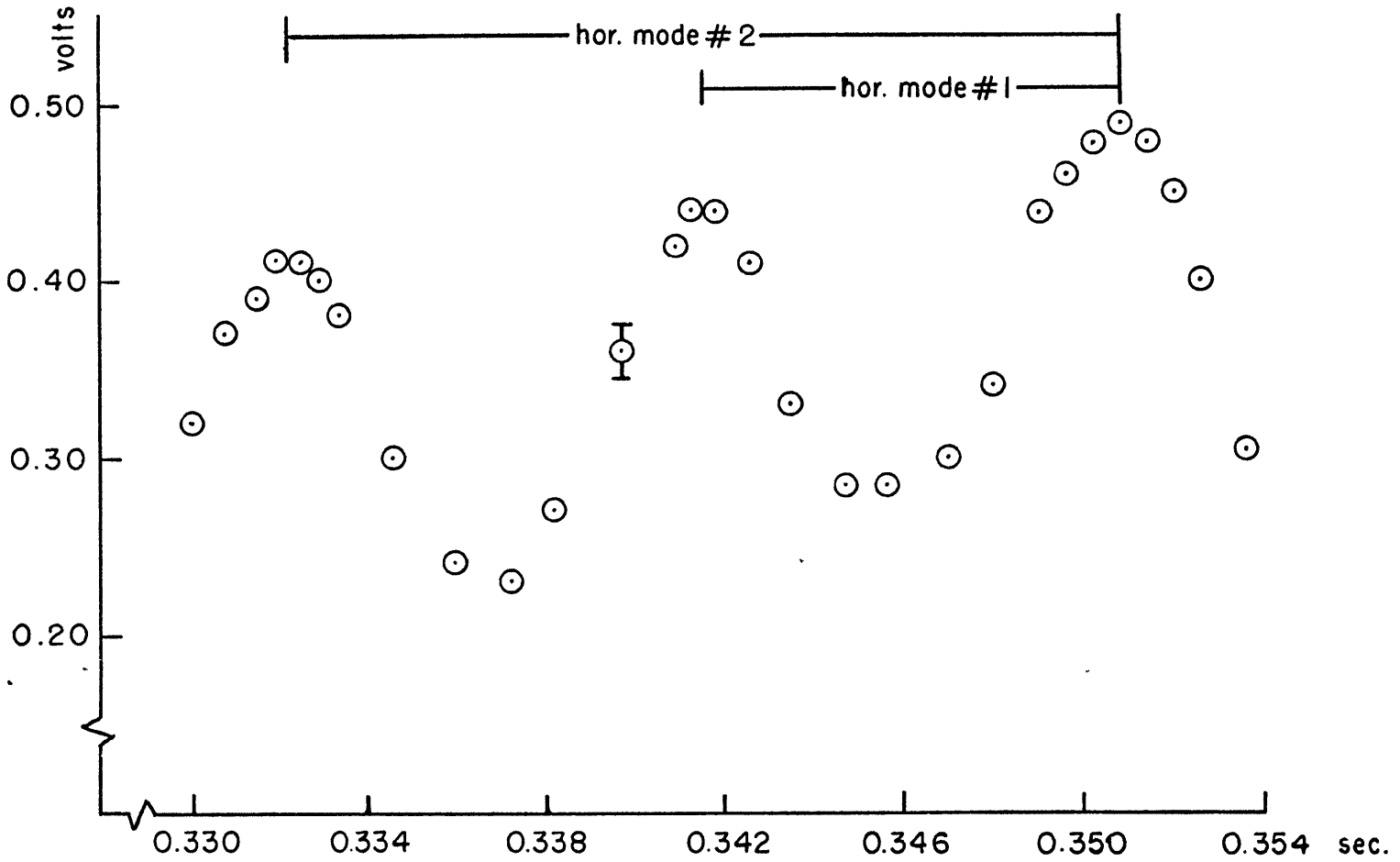

Figure II-4 Surface wave amplitude response

frequency σ_{03} existed which was approximately equal to the difference frequency of a pair of surface eigen modes. For the generation of the fundamental internal wave (horizontal mode number of 1), two neighboring surface wave peaks were selected. If the second horizontal internal mode was desired, two frequencies in the surface wave response curve were chosen so as to be separated by one peak. This is indicated in figure II-4. One of the surface eigen frequencies σ_{01} was fixed and a response curve of the internal wave was obtained by varying the second surface wave frequency σ_2 and measuring particle amplitudes. The second surface wave frequency, σ_2 was always within 0.5% of the eigen frequency.

Initial growth to "steady state" of the internal wave was measured with the pressure probe. One (or both) of the wavemaker motors was then turned off and the viscous decay of the internal wave measured in a similar way. Since surface wave viscous decay times were an order of magnitude shorter than those of the internal waves, turning the paddle off provided after only a short lapse of time an initial condition of no surface wave forcing for the internal wave. In like manner, turning the paddle on provided after only a short lapse of time an initial condition of an established surface wave field for the forcing of the resonant internal wave. The surface wave "response time" was typically one internal wave period.

Following each series of runs (each of which lasted a few hours), the density structure was measured and the probes were recalibrated. In the two layer experiments, the mean position of the interface was also

changed and the above procedure repeated.

While the linear stratifications remained usable for several days, the two-layer profiles needed to be "sharpened up" every few hours. This was accomplished by siphoning off fluid from the interface region and replacing it with fresh and salty water at the top and bottom respectively.

C. Data Analysis

The analog data from the pressure and wave probes, paddle monitor, and phase resolver for each experiment were stored on tape using a Precision Instruments (model 6108) eight track FM tape recorder. Playback in the FM mode reproduced the original signals with little distortion and permitted further analysis. During the period of resonant growth of the internal wave, data from the four sensors were played into a Sanborn 4 channel strip chart recorder (model 67-1200). Playback was usually at ten times the original tape speed. This permitted the use of two Rockland active filters (model 1010F), a Quan-Tech wave analyzer (model 304), and a PAR (Princeton Applied Research model 101) correlator. The wave analyzer computed $|\text{amplitude}|^2$ spectra of the surface and pressure probes as well as the wavemaker monitor. As it took a finite time for the sliding filter to sweep through the desired range of frequencies, spectra should be thought of as only representative of some "average" value of time for nonstationary data. When a steady state was achieved in any given experiment, the correlator was also used. Tape loops containing ten internal waves were made and the cross correlation between the pressure and resolver signals permitted a phase de-

termination. This method agreed quite well with the "direct" method of measurement from the strip chart recorder tracings.

CHAPTER III. Interfacial Theory

In this chapter the resonant interaction of two surface waves and one internal gravity wave will be discussed for the special case of a step function density profile. In the mathematical model, all waves will be assumed to be two-dimensional, standing, and irrotational except in a narrow region about the interface. Except in calculations for viscous dissipation of wave energy, this finite interface thickness will be neglected. The following three sections will contain: general formulation, derivation of interaction coefficient for the "generation" of an internal wave from two surface waves, and an analytical solution for resonant internal wave growth including viscosity and slight detuning. Derivation of the viscous decay parameter and the back interaction equations for the effect of a growing internal wave upon the surface waves may be found in the theoretical appendix. The predictions made in this chapter will be compared with experimental results in Chapter V. Several approximations are made in what follows with experimental parameters in mind.

A. Formulation

The geometry of the model is shown in figure III-1. The fluid will be considered incompressible, non-diffusive, inviscid (later to be relaxed), and irrotational away from the interface. The density difference between the constant densities of the lower and upper layers will be assumed small. Effects of surface tension will be neglected for convenience. The equations and boundary conditions are well known (see for example, Lamb § 231).

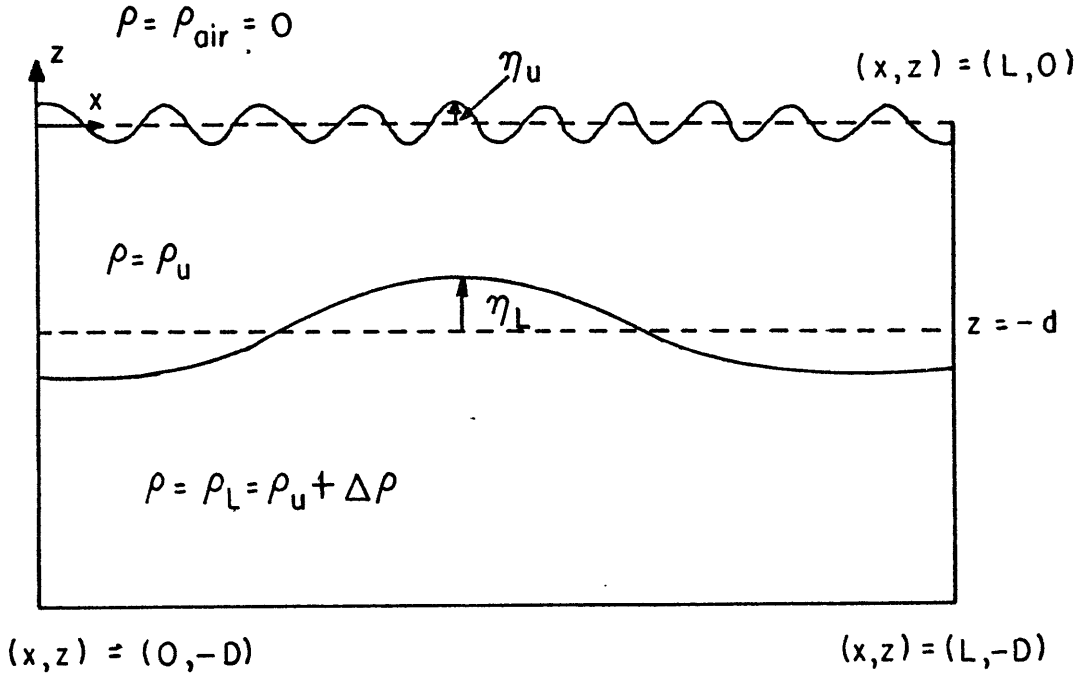

Figure III-1 Model geometry for 2-layer theory

$$u_{u,L} = \nabla \phi_{u,L} . \tag{3a.1}$$

$$\nabla^2 \phi_{u,L} = 0 . \tag{3a.2}$$

$$\left.\begin{aligned} &\frac{\partial \eta_u}{\partial t} + \nabla \phi_u \cdot \nabla \eta_u = \frac{\partial \phi_u}{\partial z} \qquad (3a.3) \\ &\frac{\partial \phi_u}{\partial t} + \tfrac{1}{2}(\nabla \phi_u)^2 + g \eta_u = 0 \qquad (3a.4) \end{aligned}\right\} z = \eta_u .$$

$$\left.\begin{aligned} &\frac{\partial \eta_L}{\partial t} + \nabla \phi_{u,L} \cdot \nabla \eta_L = \frac{\partial \phi_{u,L}}{\partial z} . \qquad (3a.5) \\ &\rho_u \frac{\partial \phi_u}{\partial t} + \tfrac{1}{2}\rho_u (\nabla \phi_u)^2 + g \rho_u \eta_u = \rho_L \frac{\partial \phi_L}{\partial t} + \tfrac{1}{2}\rho_L (\nabla \phi_L)^2 + g \rho_L \eta_L . \qquad (3a.6) \end{aligned}\right\} z = -d + \eta_L$$

$$\frac{\partial \phi_{u,L}}{\partial x} = 0 \ , \ x = 0, L \quad , \quad \frac{\partial \phi_L}{\partial z} = 0 \ , \ z = -D . \tag{3a.7}$$

The atmospheric pressure has been assumed to be zero and the arbitrary functions of time in (3a.6) have been incorporated into the velocity potentials. The set of boundary conditions will be evaluated at the mean levels of the interfaces by expanding them in Taylor series with cubic and higher order product terms neglected. Thus, (3a.3-6) become

$$\left.\begin{aligned} &\frac{\partial \eta_u}{\partial t} - \frac{\partial \phi_u}{\partial z} = \frac{\partial^2 \phi_u}{\partial z^2} \eta_u - \nabla \phi_u \cdot \nabla \eta_u \qquad (3a.8) \\ &\frac{\partial \phi_u}{\partial t} + g \eta_u = - \frac{\partial^2 \phi_u}{\partial t \partial z} \eta_u - \tfrac{1}{2}(\nabla \phi_u)^2 \qquad (3a.9) \end{aligned}\right\} z = 0 ,$$

$$\text{or} \quad \frac{\partial^2 \phi_u}{\partial t^2} + g \frac{\partial \phi_u}{\partial z} = N_1 \quad , \ z = 0 . \tag{3a.10}$$

$$(3a.11)\qquad N_1 \equiv -g\frac{\partial^2\phi_U}{\partial t^2}\eta_U + g\nabla\phi_U\cdot\nabla\eta_U - \frac{\partial}{\partial t}\left(\frac{\partial^2\phi_U}{\partial t\partial z}\eta_U\right) - \frac{1}{2}\frac{\partial}{\partial t}(\nabla\phi_U)^2 .$$

$$(3a.12)\qquad \rho_U\frac{\partial\phi_U}{\partial t} - \rho_L\frac{\partial\phi_L}{\partial t} + g(\rho_U-\rho_L)\eta_L = N_2 \quad , z=-d$$

$$(3a.13)\qquad \frac{\partial\eta_L}{\partial t} - \frac{\partial\phi_{U,L}}{\partial z} = N_3 \quad , \quad z=-d$$

$$(3a.14)\qquad N_2 \equiv \left(\rho_L\frac{\partial^2\phi_L}{\partial t\partial z} - \rho_U\frac{\partial^2\phi_U}{\partial t\partial z}\right)\eta_L + \frac{1}{2}\left[\rho_L(\nabla\phi_L)^2 - \rho_U(\nabla\phi_U)^2\right] ,$$

$$(3a.15)\qquad N_3 \equiv \frac{\partial^2\phi_{U,L}}{\partial z^2}\eta_L - \nabla\phi_{U,L}\cdot\nabla\eta_L .$$

The linear solutions of the above set of equations are discussed by Lamb (in Hydrodynamics, § 231). For

$$(3a.16)\qquad \phi_{U,L} = f_{U,L}(z)\cos\chi x\cos(\sigma t+\Theta) ,$$

with $f_{U,L}(z)$ suitably chosen to satisfy the boundary conditions (3a.7,10,12,13), one can obtain the dispersion relation or constraint between the frequency σ and the wavenumber χ. Namely,

$$(3a.17)\qquad \sigma^4[\rho_L\coth\chi(D-d)\coth\chi d+\rho_U] - \sigma^2\rho_L[\coth\chi d+\coth\chi(D-d)]g\chi + (\rho_L-\rho_U)g^2\chi^2 = 0.$$

We are going to consider solutions to the above biquadratic equation for σ which are perturbations about the following:

$$(3a.18)\qquad \sigma_{OS}^2 = g\chi$$

$$(3a.19)\qquad \sigma_{OI}^2 = (\rho_L-\rho_U)g\chi\left[\rho_L\coth\chi(D-d)+\rho_U\coth\chi d\right]^{-1}$$

Equation (3a.18) is the dispersion relation for deep water surface

gravity waves which are not affected by the stratification. The second represents the familiar rigid lid internal gravity waves. We anticipate these to be proper choices when $\Delta\rho/\bar{\rho} \ll 1$ where

$$\Delta\rho \equiv \rho_L - \rho_U \,, \quad \bar{\rho} = \tfrac{1}{2}(\rho_U + \rho_L)$$

Note that,

$$(\sigma^2 - \sigma_{0S}^2 + \delta_S)(\sigma^2 - \sigma_{0I}^2 + \delta_I) =$$

(3a.20)

$$\sigma^4 - \sigma_{0S}^2\sigma^2\left[1 - \delta_I/\sigma_{0S}^2 - \delta_S/\sigma_{0S}^2 + \left(\sigma_{0I}/\sigma_{0S}\right)^2\right] +$$

$$\sigma_{0S}^2\sigma_{0I}^2\left[1 - \delta_S/\sigma_{0S}^2 - \delta_I/\sigma_{0I}^2 + O\left\{\left(\delta_S/\sigma_{0S}^2\right)^2, \left(\delta_I/\sigma_{0S}^2\right)^2\right\}\right]$$

and rewrite (3a.17),

(3a.21)

$$\sigma^4 - \sigma^2\sigma_{0S}^2\left[\frac{\rho_L \coth\chi d + \rho_L \coth\chi(D-d)}{\rho_L \coth\chi d \coth\chi(D-d) + \rho_U}\right] + \sigma_{0S}^2\sigma_{0I}^2\left[\frac{\rho_U \coth\chi d + \rho_L \coth\chi(D-d)}{\rho_L \coth\chi d \coth\chi(D-d) + \rho_U}\right] = 0$$

It may be noticed that the terms in $[\ ]$'s above are nearly equal for $\rho_L \doteq \rho_U$. The term $\dfrac{\coth\chi d + \coth\chi(D-d)}{1 + \coth\chi d \coth\chi(D-d)} \equiv Q$ will be evaluated with representative wave numbers for $d = D-d$ and $D/L = 1/2$.

Case 1 represents an internal wave

$$\chi = \chi_{min.} = \pi/L \,, \quad L = 180\,cm.$$

$$\chi(D-d) = \chi d = \pi/4 \,, \quad Q = 0.915$$

Case 2 represents a surface wave

$$\chi = 20\pi/L \,, \quad L = 180\,cm.$$

$$\chi(D-d) = \chi d = 5\pi \,, \quad Q = 1.00$$

Comparing (3a.20) and (3a.21) for $\left(\sigma_{0I}/\sigma_{0S}\right)^2 \doteq \Delta\rho/\bar{\rho} \ll 1$, one sees that the variations δ_I, δ_S are small and the two modes of motion are essentially decoupled in the linear case. Note that the effect of a

free surface upon the internal wave, though small (< 0.1), is by no means beyond the range of experimental determination. A slight correction will have to be made at a later stage in the analysis.

With the above introduction in mind, we turn now to the nonlinear problem. As is common with quadratic wave-wave interactions, the nonlinear terms may cause a slow transfer of energy and momentum among the normal modes and higher harmonics of the system. The normal modes in the limiting case of weak stratification are simply the eigenmodes of surface standing waves with no stratification and standing, rigid lid internal waves. For the rectangular geometry in figure III-1, all wave numbers must satisfy $\chi L = n\pi$, where n is a positive integer. Quadratic products in N_1, N_2, and N_3 are of the form $\cos\chi_n x \cos\chi_m x$ and $\cos\chi_n x \sin\chi_m x$. These are expressible as sums of $\sin(\chi_m \pm \chi_n)x$ and $\cos(\chi_m \pm \chi_n)x$. It is interesting to note that if two waves in a triad of interacting waves for which $\chi_1 \pm \chi_2 \pm \chi_3 = 0$ are standing, the third member, if it exists, is automatically a standing wave. Whether or not the third member of any triad exists depends upon two additional factors, the kinematic condition that $\sigma_1 \pm \sigma_2 \pm \sigma_3 = 0$ and a non-aero interaction coefficient governing the momentum transfer among the waves of a triad. It willbe demonstrated in the next section that both of these conditions may be satisfied and that a triad exists consisting of two surface waves and one internal wave. For any two given surface waves, the kinematic conditions can be satisfied exactly by a proper choice of density difference $\Delta\rho/\bar{\rho}$, interface depth d, and total depth D. For further discussion of kinematic conditions see Thorpe (1966A).

B. Interaction coefficient and averaged inviscid resonance

Following earlier work (e.g., Simmons 1969), three primary waves satisfying the dispersion relationship $\sigma_n = \sigma_{on}(\chi_n)$, to the lowest order in the wave slope $\epsilon_n = \chi_n a_n$, are given by

$$(3b.1) \qquad \phi_n = \frac{a_n \sigma_n}{\chi_n} f_n(z) \cos \chi_n x \cos(\sigma_n t + \theta_n)$$

a_n = particle amplitude of n^{th} wave

σ_n = frequency of n^{th} wave

χ_n = wave number of n^{th} wave

$f_n(z)$ = verticle eigen function of n^{th} wave

θ_n = phase of n^{th} wave

σ_{on} = eigen frequency of n^{th} wave

The amplitude and phase are allowed to be slowly varying functions of time as caused by the resonant interaction. Both effects must be simultaneously considered for a complete solution to the problem.

A notational change at this point will now be made. ϕ_n will refer to the velocity potential of the n^{th} wave. The subscripts **U, L** for "upper" and "lower" will be dropped. It must be understood that when ϕ_n is an internal wave velocity potential evaluated at the free surface $z = 0$, it is ϕ_n^{upper} which is really being considered. Letting

$$(3b.2) \qquad \phi = \sum_{n=1}^{3} \frac{a_n \sigma_n}{\chi_n} f_n(z) \cos \chi_n x \cos(\sigma_n t + \theta_n)$$

$$(3b.3) \qquad \eta = \sum_{n=1}^{3} \frac{a_n \sigma_n^2}{g \chi_n} f_n(0) \cos \chi_n x \sin(\sigma_n t + \theta_n),$$

then $\frac{d^2 f_n}{dz^2} - \chi_n^2 f = 0$ and f_n satisfies the appropriate boundary conditions.

Inserting (3b.2) into (3a.11) gives

$$(3b.4) \quad N_1 = \frac{1}{4} \sum_{\substack{i,j \\ i \le j}}^{3} \frac{a_i a_j \sigma_i \sigma_j}{\chi_i \chi_j} \Big\{ -r \sigma_j f_i'' f_j - \sigma_i f_i f_j''$$

$$- \chi_i f_i \chi_j f_j (r \cdot s \sigma_j + s \sigma_i) + r \frac{(\sigma_i + r\sigma_j)}{g} \sigma_i \sigma_j (f_i' f_j +$$

$$f_j' f_i) + (\sigma_i + r\sigma_j)(-s \chi_i \chi_j f_i f_j + f_i' f_j') \Big\} *$$

$$\cos(\chi_i + s\chi_j) x \sin(\overline{\sigma_i + r\sigma_j}\, t + \theta_i + r\theta_j) \quad , z = 0$$

with $r, s = \pm 1.$

We have calculated the general form of one of the three nonlinear terms in the equations of motion, N_1 . It arises from the dynamic boundary condition at the upper surface. When one or more waves in any given triad is a surface wave, a great simplification in the algebra is possible providing the interface is sufficiently below the upper surface (e.g., $\chi_{surf} d > \pi$). Since the nonlinear terms N_2 and N_3 involve at least one surface eigen function evaluated at $z = -d$, the direct forcing of an internal wave by surface waves through the

interfacial boundary condition is negligible compared to forcing at the upper surface. A similar result can be found in the next chapter for the interaction of two surface waves and one internal wave in a slowly varying stratification. In this section, the validity of this assertion will be shown a posteriori in equation (3b.33).

We will now evaluate the nonlinear term N_1 for the particular case in which initially only two waves are present and both of these are surface waves. A substitution will be made which will transfer the nonlinear term N_1 from the surface boundary condition to the interfacial boundary condition where it can be compared with the other nonlinear terms arising from the two surface waves.

If ϕ_1 and ϕ_2 represent two surface waves and ϕ_3 a mode whose type is to be determined, then substituting $\phi = \phi_1 + \phi_2 + \phi_3$ into the equations gives,

$$(3b.5) \qquad \left(\frac{\partial^2}{\partial t^2} + g\frac{\partial}{\partial z}\right)(\phi_1+\phi_2+\phi_3) = N_1(\phi_i,\phi_j), \quad z = 0,$$

$$(3b.6) \qquad \rho^U \frac{\partial \phi_3^U}{\partial t} - \rho^L \frac{\partial \phi_3^L}{\partial t} + g(\rho^U - \rho^L)\eta^L = N_2$$

$$(3b.7) \qquad \frac{\partial \eta^L}{\partial t} - \frac{\partial \phi_3^{U,L}}{\partial z} = N_3, \qquad \Big\} \; z = -d,$$

$$(3b.8) \qquad \frac{\partial \phi_3}{\partial z} = 0, \quad z = -D,$$

$$(3b.9) \qquad \nabla^2 \phi_3 = 0.$$

As mentioned earlier, the effect of nonlinear terms upon the surface modes will be discussed in the appendix. It will be seen that most of the experimental results can be explained under the assumption that the surface waves remain constant. This assumption will be discussed later. Thus,

$$(3b.10) \qquad \left(\frac{\partial^2}{\partial t^2} + g\frac{\partial}{\partial z}\right)(\phi_1 + \phi_2) = 0 \quad , z = 0$$

$$(3b.11) \qquad \left(\frac{\partial^2}{\partial t^2} + g\frac{\partial}{\partial z}\right)\phi_3 = N_1(\phi_1, \phi_2) \quad , z = 0$$

Making the substitution, $\phi_3 = \varphi_3 + \tilde{\varphi}$, one has

$$(3b.12) \qquad \frac{\partial^2 \varphi_3}{\partial t^2} + g\frac{\partial \varphi_3}{\partial z} = N_1 - \left(\frac{\partial^2 \tilde{\varphi}}{\partial t^2} + g\frac{\partial \tilde{\varphi}}{\partial z}\right), \quad z = 0,$$

$$(3b.13) \qquad \rho^u \frac{\partial \varphi_3^u}{\partial t} - \rho^\ell \frac{\partial \varphi_3^\ell}{\partial t} + g(\rho^u - \rho^\ell)\eta^\ell = N_2 - \left(\rho^u \frac{\partial \hat{\varphi}}{\partial t} - \rho^\ell \frac{\partial \hat{\varphi}}{\partial t}\right), \quad z = -d$$

$$(3b.14) \qquad \frac{\partial \varphi_3}{\partial z} + \frac{\partial \hat{\varphi}}{\partial z} = 0 \quad , z = -D$$

$$(3b.15) \qquad \nabla^2 \varphi_3 + \nabla^2 \tilde{\varphi}_3 = 0$$

$$(3b.16) \qquad \frac{\partial \eta^\ell}{\partial t} - \frac{\partial \varphi_3^{u,\ell}}{\partial z} = N_3 + \frac{\partial \hat{\phi}}{\partial z} \quad , z = -d$$

The function $\tilde{\phi}$ will be chosen so as to satisfy the following equations:

(3b.17) $$\frac{\partial^2 \tilde{\phi}}{\partial t^2} + g \frac{\partial \tilde{\phi}}{\partial z} = N_1(\phi_1, \phi_2) \quad , z=0 \ ,$$

(3b.18) $$\frac{\partial \tilde{\phi}}{\partial z} = 0 \quad , z=-D,$$

(3.b.19) $$\nabla^2 \tilde{\phi} = 0$$

This gives for ϕ_3 ,

(3b.20) $$\left(\frac{\partial^2}{\partial t^2} + g \frac{\partial}{\partial z}\right) \phi_3 = 0 \quad , z=0$$

(3b.21) $$\frac{\partial \phi_3}{\partial z} = 0 \quad , z=-D$$

(3b.22) $$\nabla^2 \phi_3 = 0$$

The function $\tilde{\phi}$ is given by

(3b.23) $$\tilde{\phi} = \frac{1}{4} \sum_{\substack{i,j \\ i \neq j}}^{2} \frac{+ \frac{a_i a_j \sigma_i \sigma_j}{x_i x_j} \{\ \}}{g\tilde{x} \sinh \tilde{x} D \left(1 - \frac{\tilde{\sigma}^2}{g\tilde{x}} \coth \tilde{x} D\right)} *$$

$$\cos \tilde{x} x \sin(\tilde{\sigma} t + \tilde{\theta}) \cosh \tilde{x}(z+D) \ , \begin{matrix} r = \pm 1 \\ s = \pm 1 \end{matrix}$$

where

$$\tilde{x} = x_i + s x_j$$

(3b.24)
$$\tilde{\sigma} = \sigma_i + r \sigma_j$$

$$\tilde{\theta} = \theta_i + r \theta_j$$

and $\{\ \}$ is given in (3b.4). $\tilde{\Phi}$ can be interpreted as a "forced

harmonic" surface wave. Since the original two waves were deep water surface waves, it is not possible for the denominator in (3b.23) to vanish. This is merely a statement that resonant interactions among only deep water surface waves are not possible because the kinematic conditions for resonance cannot be satisfied at this order.

The equations (3b.13, 3b.14, 3b.20, 3b.21, 3b.22) are the equations governing a possible internal wave ϕ_3 which is being forced by known nonlinear terms which appear only in the interfacial boundary conditions. We have seen that for a small density difference, the rigid top boundary condition is a good approximation. Suppose ϕ_3 represents a rigid lid internal wave. Thus,

$$\phi_3^U = \frac{a_3\sigma_3}{\chi_3}\cosh\chi_3 z\cos\chi_3 x\cos(\sigma_3 t+\theta_3)$$

(3b.25)

$$\phi_3^L = -\frac{a_3\sigma_3}{\chi_3}\frac{\sinh\chi_3 d}{\sinh\chi_3(D-d)}\cosh\chi_3(z+D)\cos\chi_3 x\cos(\sigma_3 t+\theta_3)$$

Using (3a.19), substituting (3b.25) into (3b.13), and eliminating η^L by using (3b.14) one gets,

$$\left(\frac{\partial^2}{\partial t^2}+\sigma_{03}^2\right)\left[\frac{a_3\sigma_3}{\chi_3}\cos\chi_3 x\cos(\sigma_3 t+\theta_3)\right] = +\sigma_{03}^2 N_T,\quad z=-d, \tag{3b.26}$$

where

$$N_T = \frac{g\Delta\rho\frac{\partial\bar{\phi}}{\partial z}+\Delta\rho\frac{\partial^2\bar{\phi}}{\partial t^2}+\frac{\partial N_2}{\partial t}+g\Delta\rho N_3}{g\chi_3\Delta\rho\sinh\chi_3 d} \tag{3b.27}$$

For slowly varying amplitudes and phases (i.e., for $\frac{1}{a_j}\frac{\partial a_j}{\partial t}$, $\frac{\partial\theta_j}{\partial t}$,

$\ll \sigma_j$, $j = 1, 2, 3$), the left-hand side of (3b.26) can be rewritten using

$$\frac{\partial^2}{\partial t^2}\left[\left(\frac{a_3\sigma_3}{\chi_3}\right)\cos\chi_3 x \cos(\sigma_3 t+\theta_3)\right] =$$

$$-\frac{a_3\sigma_3}{\chi_3}\cos\chi_3 x\left\{\left[(\sigma_3+\frac{\partial\theta}{\partial t})^2-\frac{1}{a}\frac{\partial^2 a}{\partial t^2}\right]\cos(\sigma_3 t+\theta_3)+\right.$$

$$\left.\left[\frac{\partial^2\theta_3}{\partial t^2}+2\left(\sigma_3+\frac{\partial\theta_3}{\partial t}\right)\frac{1}{a_3}\frac{\partial a_3}{\partial t}\right]\sin(\sigma_3 t+\theta_3\right\} =$$

$$-\frac{a_3\sigma_3^3}{\chi_3}\cos\chi_3 x\left\{\left[1+2\frac{\partial\theta_3}{\partial t}\right]\cos(\sigma_3 t+\theta_3)+\left[2/\sigma_3/a_3\frac{\partial a_3}{\partial t}\right]\sin(\sigma_3 t+\theta_3)\right\}$$

$$+ o\left[\left(\frac{a_{3tt}}{\sigma_3^2 a_3}\right),\left(\frac{a_{3t}\theta_{3t}}{a_3\sigma_3}\right),\left(\frac{\theta_{3t}}{\sigma_3}\right)^2\right]$$

Thus (3b.26) becomes

$$-\frac{\sigma_3 a_3}{\chi_3}\cos\chi_3 x\left\{\left[\sigma_3^2-\sigma_{03}^2+2\sigma_3\frac{\partial\theta_3}{\partial t}\right]\cos(\sigma_3 t+\theta_3)+\right.$$

$$\left.2\sigma_3\frac{1}{a_3}\frac{\partial a_3}{\partial t}\sin(\sigma_3 t+\theta_3)\right\} + h.o.t. \tag{3b.28}$$

$$= \sigma_{03}^2 N_T$$

In the absence of nonlinear terms the left-hand side of (3b.28) reduces to $\frac{\partial\theta_3}{\partial t} = \frac{\partial a_3}{\partial t} = 0$, $\sigma_3^2 = \sigma_{03}^2$. The nonlinearities cause changes in all of the above quantities. One can estimate from (3b.28) and (3b.23) that

$$a_3\frac{\partial\theta_3}{\partial t}, \frac{\partial a_3}{\partial t} \sim (\chi_1 a_1 \cdot \chi_2 a_2)^{1/2}(a_1 \cdot a_2)^{1/2}\sigma_3 \tag{3b.29}$$

One can see that for small surface wave slopes, $\epsilon_1 = \chi_1 a_1$, $\epsilon_2 = \chi_2 a_2$, the time derivatives in (3b.28) of the amplitude and phase are small compared to the explicit time derivatives of the trigonometric quantities $\cos(\sigma_3 t + \theta_3)$. The type of system represented in (3b.28) has been studied in detail in standard texts on nonlinear mechanics. We will use the "method of averaging" discussed in Bogoliubov and Mitropolsky (1961) to obtain equations for the slow amplitude and phase modulation. To obtain these equations multiply both sides of (3b.28) successively by $\cos\chi_3 x \cos(\sigma_3 t + \theta_3)$ and $\cos\chi_3 x \sin(\sigma_3 t + \theta_3)$ and integrate over one wave period $\frac{2\pi}{\sigma_3}$ and the length of the tank, L. In the integration over space and time, time variations of the amplitudes and phases may be ignored. For example

$$\int_{-\frac{\pi}{\sigma_3}}^{\frac{\pi}{\sigma_3}} dt \frac{\partial a_3}{\partial t} \sin^2(\sigma_3 t + \theta_3) \sim \frac{\pi}{\sigma_3} \frac{\partial a_3}{\partial t}.$$

The same sort of result can be obtained in a "cleaner" fashion using a two-time expansion. The answer is the same either way. Remembering that $\chi_1 = \frac{n_1\pi}{L}$, $\chi_2 = \frac{n_2\pi}{L}$ and $\chi_3 = \frac{n_3\pi}{L}$ one obtains the following equations.

(3b.30)
$$2 a_3 \sigma_3^2 \frac{\partial \theta_3}{\partial t} + (\sigma_{03}^2 - \sigma_3^2) a_3 \sigma_3 =$$
$$- \sigma_{03}^2 \left(\frac{\chi_3}{\sigma_3}\right)\left(\frac{\sigma_3}{\pi}\right)\left(\frac{2}{L}\right) \int_{-\pi/\sigma_3}^{\pi/\sigma_3} dt \int_0^L dx \, N_T \cos\chi_3 x \cos(\sigma_3 t + \theta_3)$$

$$2\frac{\partial a_3}{\partial t}\sigma_3^2 = -\sigma_{03}^2\left(\frac{\chi_3}{\sigma_3}\right)\left(\frac{\sigma_3}{\pi}\right)\left(\frac{2}{2}\right)\int dt\int dx\, N_T \cos\chi_3 x \sin(\sigma_3 t+\theta_3) \tag{3b.31}$$

The integration over x can be carried out immediately with the result,

$$2a_3\sigma_3^2\frac{\partial\theta_3}{\partial t} + (\sigma_{03}^2-\sigma_3^2)a_3\sigma_3 = \begin{cases}\cos(\sigma_3 t+\theta_3)\\ \sin(\sigma_3 t+\theta_3)\end{cases} -\sigma_{03}^2\left(\frac{\chi_3}{\pi}\right)\delta_{k\ell}(\chi_3-\tilde{\chi})\int dt\, N_T \tag{3b.32}$$

$$2\sigma_3^2\frac{\partial a_3}{\partial t} = \begin{cases}\cos(\sigma_3 t+\theta_3)\\ \sin(\sigma_3 t+\theta_3)\end{cases} -\sigma_{03}^2\left(\frac{\chi_3}{\pi}\right)\delta_{k\ell}(\chi_3-\tilde{\chi})\int dt\, N_T \tag{3b.33}$$

$$\delta_{k\ell}(\chi_3-\tilde{\chi}) = \begin{cases} 1 & , \chi_3=\tilde{\chi} \\ 0 & , \chi_3\neq\tilde{\chi}\end{cases} \tag{3b.34}$$

The integration over time can be carried out following the ordering scheme developed by Bogoliubov and Mitropolsky (1961). The lowest order iteration gives only the contribution due to forcing frequencies equal to the frequency of the internal wave, σ_3. These side conditions on the wave number χ_3 and frequency σ_3 are just the kinematic resonance conditions $\chi_i + \rho\chi_j - \chi_3 = 0$, $\sigma_i + \gamma\sigma_j - \sigma_3 = 0$, $\gamma, \rho = \pm 1$.

If σ_3 is to be near an eigen frequency of a free internal wave σ_{03}, then for comparable wavenumbers, σ_3 must be much smaller than σ_1, σ_2 in order that the internal and surface modes are sufficiently decoupled for the rigid lid boundary condition to be used. In the experiments $\sigma_3/\sigma_1 \doteq \sigma_3/\sigma_2 \doteq .03$ and $\chi_3/\chi_1 \doteq \chi_3/\chi_2 \doteq 0.1$. Thus, we are

interested in the case in which $r=s=-1$. Other combinations of frequencies and wavenumbers of the surface waves will not produce a forcing commensurate with that of a free internal wave. Because of the disparity between the frequencies and wavenumbers of the surface and internal waves, it is possible to show that only the first nonlinear term in (3b.27) contributes to the interaction. In fact,

$$(3b.35)\quad \frac{|N_2|}{\left|\Delta\rho \frac{\partial \tilde{\phi}}{\partial t}\right|} \sim \frac{|N_3|}{\left|\frac{\partial \tilde{\phi}}{\partial t}\right|} \sim \frac{\exp[-(\chi_1+\chi_2)d]}{\sinh[(\chi_1-\chi_2)(D-d)]} << 1$$

and

$$\frac{\tilde{\sigma}^2}{g\tilde{\chi}\tanh\tilde{\chi}D} << 1.$$

Under the above restrictions and the requirement that χ_3 and σ_3 always be positive, equations (3b.32) and (3b.33) reduce to

$$(3b.36)\quad a_3\frac{\partial\theta_3}{\partial t} + \frac{1}{2}\left[1-\left(\frac{\sigma_{03}}{\sigma_3}\right)^2\right]a_3\sigma_3 = -I\sin(\theta_1-\theta_2-\theta_3),$$

$$(3b.37)\quad \frac{\partial a_3}{\partial t} = -I\cos(\theta_1-\theta_2-\theta_3),$$

where

$$(3b.38)\quad I = \frac{(a_1\sigma_1)(a_2\sigma_2)\sinh\chi_3(D-d)}{2g\sinh\chi_3 D\sinh\chi_3 d}\sigma_3$$

and

$$\sigma_1-\sigma_2-\sigma_3=0$$
$$\chi_1-\chi_2-\chi_3=0$$

In deriving the above equations, (3b.4) has been used with

$f_1(z) = \exp \chi_1 z$, $f_2(z) = \exp \chi_2 z$, $\sigma_1^2 = g\chi_1$, $\sigma_2^2 = g\chi_2$ and $\alpha = -1 = r$, $i = 1, j = 2$. It has not been assumed that $\sigma_3^2 = \sigma_{03}^2$. Instead a slight amount of detuning, δ , will be permitted such that $\sigma_3 = \sigma_{03}(1+\delta)$, $\delta << 1$. Equation (3b.36) becomes to lowest order in δ and $\epsilon = (\epsilon_1 \epsilon_2)^{1/2}$,

$$(3b.39) \qquad a_3 \frac{\partial \theta_3}{\partial t} + \delta \sigma_3 a_3 = -I \sin(\theta_1 - \theta_2 - \theta_3).$$

C. Viscosity included

Following the lead of McGoldrick (1965, 1970), McKewan (1971), and Kim and Hanratty (1971), each mode is assumed to decay independently. An unforced mode n will decay at a rate $\dot{a}_n / a_n = -\lambda_n$. The decay factor λ_n is independent of amplitude a_n and depends upon viscosity, wavelength, frequency, and the geometry of the tank. The primary source of viscous dissipation for the parameters used in the laboratory experiment is due to side wall boundary layers. The decay factor can be found experimentally and theoretically. For the purpose of this section, λ_n will be a known constant for any given mode. Further discussion of λ_n will be found in Chapter V and the general appendix.

In order to be consistant with earlier approximations, the fluid must be only slightly viscous. ($\lambda_n / \sigma_n << 1$). The equations of the previous section can be modified to include viscosity. Note that viscosity affects only the amplitude equation and not the phase equation,

so that

$$(3c.1) \qquad a_3 \frac{\partial \theta_3}{\partial t} + \delta\nabla_3 a_3 = -I \sin(\theta_1 - \theta_2 - \theta_3)$$

$$(3c.2) \qquad \frac{\partial a_3}{\partial t} + \lambda_3 a_3 = -I \cos(\theta_1 - \theta_2 - \theta_3)$$

The properties of this pair of equations will be investigated for the special case in which surface wave amplitudes a_1, a_2 and phases θ_1, θ_2 are constant for all time, but a_3 and θ_3 are allowed to vary with time. In previous work with nonlinear interactions, this approximation is valid only in the initial stages of the interaction. For later times one must consider the back interaction equations (see general appendix) and other higher order effects. In the experiments conducted, it was found that this approximation suffices for all times <u>if</u> the amplitude of the internal wave remains small.

Under the above restrictions, (3c.1) and (3c.2) become

$$(3c.3) \qquad a \frac{d\theta}{dt} + \delta\nabla_3 a = I \sin\theta$$

$$(3c.4) \qquad \frac{da}{dt} + \lambda a = -I \cos\theta$$

where

$$(3c.5) \qquad a = a_3 \,, \; \lambda = \lambda_3 \,, \; \theta = \theta_3 - \theta_1 + \theta_2 \,, \; I = \text{const.};$$

$$\frac{\partial}{\partial t} \rightarrow \frac{d}{dt}$$

The full equations (3c.3) and (3c.4) will be solved exactly, but first a few illuminating special uses will be considered.

i] tuned ($\delta=0$), inviscid ($\lambda=0$) growth

$$\left.\begin{aligned} a\frac{d\theta}{dt} &= I\sin\theta, \\ \frac{da}{dt} &= -I\cos\theta, \end{aligned}\right\} \quad \frac{d}{dt}[a\sin\theta]=0.$$

If $a(0)=0$, then $a\sin\theta=0$.

For non-vanishing $\hat{a}$, $\theta=0,\pi$.

For resonant growth, $\theta=\pi$, $a=It$.

ii] tuned ($\delta=0$), viscous growth

$$a\frac{d\theta}{dt} = I\sin\theta,$$

$$\frac{da}{dt}+\lambda a = -I\cos\theta,$$

or

$$\frac{d}{dt}[ae^{\lambda t}\sin\theta]=0.$$

As before for a non-trivial solution, $\theta=0,\pi$. For resonant growth, $\theta=\pi$, so that $a=I/\lambda(1-e^{-\lambda t})$. Viscosity has no effect on the phase angle θ, but it limits the amplitude of the resonant wave.

iii] detuned, inviscid $(\lambda=0)$ growth

$$a\frac{d\theta}{dt}+\delta\nabla a = I\sin\theta,$$

$$\frac{da}{dt} = -I\cos\theta,$$

or

$$\frac{d}{dt}\left[a\sin\theta-\frac{\delta\nabla}{2I}a^2\right]=0.$$

For resonant growth with $a(0)=0$, $\theta(0)=\pi$, so that

$$a\sin\theta = \frac{\delta\nabla}{2I}a^2,$$

$$a^2\left(\theta_t+\frac{\delta\nabla}{2}\right)=0,$$

$$\Theta = \pi - \frac{\delta\sigma}{2} t ,$$

and $$a = I t \, \frac{\sin \frac{\delta\sigma}{2} t}{\frac{\delta\sigma}{2} t} .$$

(iv) steady state $\left(\frac{d}{dt} = 0\right)$, detuned and viscous

$$a = \frac{I}{\delta\sigma} \sin\Theta ,$$

$$a = -\frac{I}{\lambda} \cos\Theta .$$

For the steady state, viscously limited wave,

$$\Theta - \pi = \tan^{-1}\left(-\frac{\delta\sigma}{\lambda}\right),$$

$$a = \frac{I}{\sqrt{\lambda^2 + (\delta\sigma)^2}} .$$

(v) viscous and detuned

$$a \frac{d\theta}{dt} + \delta\sigma a = I \sin\theta ,$$

$$\frac{da}{dt} + \lambda a = -I \cos\theta .$$

Define $$x = a e^{\lambda t} \cos\theta ,$$

$$y = a e^{\lambda t} \sin\theta .$$

Then $$\frac{d^2 y}{dt^2} + (\delta\sigma)^2 y = I \delta\sigma e^{\lambda t} .$$

The solutions satisfying the initial conditions, $a(0) = 0$, $\theta(0) = \pi$ are

(3c.6) $$a = a_0 \left[1 + e^{-2\lambda t} - 2 e^{-\lambda t} \cos \delta\sigma t\right]^{1/2} ,$$

$$(3c.7)\qquad \tan(\theta-\pi) = \tan(\theta_0-\pi)\left[\frac{1-e^{-\lambda t}\cos\delta\sigma t - \frac{\lambda}{\delta\sigma}e^{-\lambda t}\sin\delta\sigma t}{1-e^{-\lambda t}\cos\delta\sigma t + \frac{\delta\sigma}{\lambda}e^{-\lambda t}\sin\delta\sigma t}\right],$$

$$(3c.8)\qquad a_0 = \frac{I}{\sqrt{\lambda^2+(\delta\sigma)^2}}$$

$$(3c.9)\qquad \tan(\theta_0-\pi) = -\frac{\delta\sigma}{\lambda}$$

Note in the limit as $\lambda \to 0$,

$$\theta \to \pi - \frac{\delta\sigma}{2}t,$$

$$a \to It\,\frac{\sin\frac{\delta\sigma}{2}t}{\frac{\delta\sigma}{2}t}.$$

In the limit as $\delta \to 0$,

$$\theta \to \pi,$$

$$a \to I/\lambda\,(1-e^{-\lambda t}).$$

In the limit as $t \to \infty$

$$\theta-\pi \to \tan^{-1}\left(-\frac{\delta\sigma}{\lambda}\right),$$

$$a \to \frac{I}{\sqrt{\lambda^2+(\delta\sigma)^2}}$$

Thus, equations (3c.6) and (3c.7) contain all of the special cases i) → iv)

The tuned inviscid growth of the interface amplitude $b_3 = a_3 \sinh \kappa_3 d$ is of the form

$$\frac{db_3}{dt} = \frac{a_1\sigma_1 a_2\sigma_2\sigma_3}{2g}\,\frac{\sinh\gamma_3(D-d)}{\sinh\gamma_3 D}\,.$$

For $\gamma_3 D \gg 1$, this becomes

$$\frac{db_3}{dt} = \frac{1}{2}\sigma_3(\gamma_1\gamma_2)^{-1/2}(\gamma_1 a_1)(\gamma_2 a_2)\exp\left[-|k_1-k_2|d\right].$$

Thorpe (1966B) obtained a similar solution for the initial growth rate of an interfacial wave resonantly "forced" by two deep water surface gravity waves, all waves being <u>progressive</u>. His result was

$$\frac{db_3}{dt} = \frac{1}{2}(1+\cos\alpha)\sigma_3(\gamma_1\gamma_2)^{-1/2}(\gamma_1 a_1)(\gamma_2 a_2)\exp\left[-|k_1-\gamma_2|d\right],$$

where $\cos\alpha = \dfrac{\vec{\gamma}_1\cdot\vec{\gamma}_2}{\gamma_1\gamma_2}$.

This result is equal to that for standing waves if $\alpha = \frac{\pi}{2}$. It is interesting to note that for colinear progressive waves (i.e., $\alpha = 0, \pi$), no interaction is predicted by Thorpe. Kinematic conditions cannot be satisfied for $\alpha = 0$, and the interaction coefficient vanishes for $\alpha = \pi$.

CHAPTER IV. Continuous Stratification Theory

In this chapter, the resonant interaction of two surface waves and one internal gravity wave will be discussed for a general stratification. The interaction coefficient and growth rate solution including detuning and viscous dissipation will be derived from a model in which all waves are assumed to be two dimensional and standing. Much of the formalism has already been presented in the previous chapter and will be used extensively whenever possible. In order to make the results of this chapter applicable to experiments conducted, the special case of a constant Brunt-Väisälä frequency will be considered. Solutions for resonant internal wave growth will as before be valid when the surface wave field remains unaffected by the presence of an internal wave. The dominant interaction term and the form of the viscous decay parameter can be found in the theoretical appendix. Predictions made in this chapter will be compared with experimental results in Chapter V.

A. Formulation

The model geometry is identical to that shown in figure III-1 except that the mean density field $\rho_0(z)$ will vary slowly and smoothly with depth. The Boussinesq approximation will be made and the effects of surface tension will be neglected. Effects of viscosity will initially be neglected as well. The equations of motion and boundary conditions are well known.

$$\frac{D\underline{u}_T}{Dt} + \frac{1}{\rho_0}\nabla P_T + g\frac{\rho_T}{\rho_0} = 0. \qquad (4a.1)$$

$$\frac{D\rho_T}{Dt} = 0 \quad , \tag{4a.2}$$

$$\nabla \cdot \underline{u} = 0 \, . \tag{4.a3}$$

If the "zeroth order" state is one of rest, then

$$\begin{aligned} \underline{u}_T &= \underline{u} \quad , \\ \rho_T &= \rho_0(z) + \rho \, , \\ P_T &= P_0 + p \quad , \quad \frac{\partial P_0}{\partial z} = -\rho_0 g \end{aligned} \tag{4.a4}$$

and the equations for the perturbations become

$$\frac{D\underline{u}}{Dt} + \frac{1}{\rho_0}\nabla p + \underline{g}\frac{\rho}{\rho_0} = 0 \, , \tag{4.a5}$$

$$\frac{D\rho}{Dt} + w\frac{\partial \rho_0}{\partial z} = 0 \, , \tag{4a.6}$$

$$\nabla \cdot \underline{u} = 0 \, . \tag{4a.7}$$

The inviscid boundary conditions imposed are

$$P_T = P_0 + p = P_{ATMOS.} = 0 \quad , \; z = \eta \, , \tag{4a.8}$$

$$\frac{D\eta}{Dt} = w \quad , \; z = \eta \tag{4a.9}$$

$$\begin{aligned} w &= 0 \quad , \; z = -D \\ u &= 0 \quad , \; x = 0, L \end{aligned} \tag{4a.10}$$

The boundary conditions at the free surface can be expanded in Taylor series about Z=0. Following Thorpe (1966A), the equations and boundary conditions (4a.5-10) can be put into the following form,

$$(4a.11)\qquad \left\{\left(\frac{\partial^2}{\partial x^2}+\frac{\partial^2}{\partial z^2}\right)\frac{\partial^2}{\partial t^2}+N^2\frac{\partial^2}{\partial x^2}\right\}w=\eta_1 \quad , \quad N^2=-\frac{g}{\rho_0}\frac{\partial \rho_0}{\partial z} \ ,$$

$$(4a.12)\qquad \left\{\frac{\partial^2}{\partial t^2}\frac{\partial}{\partial z}-g\frac{\partial^2}{\partial x^2}\right\}w=\eta_2 \quad , \quad z=0 \ ,$$

with

$$(4a.13)\qquad \begin{aligned} w &= 0 \quad , \ z=0 \ , \\ u &= 0 \quad , \ x=0,L \ , \end{aligned}$$

where

$$(4a.14)\qquad \eta_1 \equiv \frac{g}{\rho_0}\frac{\partial^2}{\partial x^2}(\underline{u}\cdot\nabla)\rho-\frac{\partial^2}{\partial x\partial t}\left[\frac{\partial}{\partial x}(\underline{u}\cdot\nabla)w-\frac{\partial}{\partial z}(\underline{u}\cdot\nabla)u\right] \ ,$$

$$(4a.15)\qquad \eta_2 \equiv \frac{\partial^2}{\partial x\partial t}(\underline{u}\cdot\nabla)u+g\frac{\partial^2}{\partial x^2}\left[\eta\frac{\partial w}{\partial z}-u\frac{\partial \eta}{\partial x}-\frac{\partial}{\partial t}\left(\eta\frac{\partial \phi}{\partial z}\right)\right] ,$$

$$(4a.16)\qquad \phi \equiv \frac{p}{g\rho_0} \ .$$

In (4a.15) higher than quadratic order product terms of perturbation quantities have been neglected. Wavelike solutions will be sought of the form $w_j = a_j \sigma_j f_j(z) \cos\chi_j x \cos(\sigma_j t + \theta_j)$.

The linear solutions of the preceeding equations have been studied by many investigators (see for example Kraus (1966)). Both a surface mode with a maximum of velocity at the free surface and an infinite number of internal modes with maximums of vertical velocity below the free surface are possible. If the parameter $N^2/g\gamma_j << 1$ where $\gamma_j^2 \equiv \chi_j^2 \left(\frac{N^2(z)}{\sigma_j^2} - 1 \right)$ is the eigenvalue of $\frac{d^2 f_j}{dz^2} + \gamma_j^2 f_j = 0$, then the upper boundary condition for internal waves consistent with the Boussinesq approximation becomes

(4a.17) $$w = 0 \quad , z = 0.$$

If the variation of density with depth had been retained in the inertial terms of (4a.1), then the full boundary condition

(4a.18) $$\left\{ \frac{\partial^2}{\partial t^2} \frac{\partial}{\partial z} - g \frac{\partial^2}{\partial x^2} \right\} w = 0 \quad , z = 0$$

would have to be used. This more difficult problem in which the eigen value appears in a boundary condition problem is discussed by Yih (1965).

If now the surface wave frequencies are much larger than the maximum Brunt-Väisälä frequency $\left(\sigma_s^2 / N_{max}^2 >> 1 \right)$, then

the effectively deep water surface waves are not affected by the stratification. Hence for linear solutions to (4a.11) and (4a.12) of the form $w_j = a_j \sigma_j f_j(z) \cos \chi_j x \cos(\sigma_j t + \theta_j)$, one may write

$$u_j = -\frac{a_j \sigma_j}{\chi_j} f_j'(z) \sin \chi_j x \cos(\sigma_j t + \theta_j), \quad f' \equiv \frac{df}{dz},$$

$$\phi_j = \frac{a_j \sigma_j^2}{g \chi_j^2} f_j'(z) \cos \chi_j x \sin(\sigma_j t + \theta_j), \tag{4a.19}$$

$$\eta_j = a_j f_j(0) \cos \chi_j x \sin(\sigma_j t + \theta_j),$$

where

$$f_j'' + \gamma_j^2 f_j = 0 \tag{4a.20}$$

$$f_j(0) = 0 \qquad \text{for an internal wave,} \tag{4a.21}$$

$$\gamma_j^2 = -\chi_j^2 \qquad \text{for a surface wave,} \tag{4a.22}$$

$$\gamma_j^2 = \chi_j^2 \left(\frac{N^2(z)}{\sigma_j^2} - 1 \right) \qquad \text{for an internal wave.} \tag{4a.23}$$

B. Interaction coefficient and inviscid resonance

Following the method used in the previous chapter, solutions consisting of triads of waves are sought. Each wave will satisfy to lowest order the linear governing equations of the previous section. Nonlinear

terms η_1 and η_2 will cause a slow modulation of the amplitudes and phases. Frequencies σ_j and wavenumbers χ_j will satisfy $\sigma_1 \pm \sigma_2 \pm \sigma_3 = 0$ and $\chi_1 \pm \chi_2 \pm \chi_3 = 0$, with $j = 1, 2$ referring to surface waves and $j = 3$ an internal wave. The results of this section will differ from those of the previous chapter in that while integrating the nonlinear terms during the "averaging" process, an additional integration in z will be necessary.

If initially two surface waves are present, then the equations for an internal wave are

$$(4b.1)\qquad \left\{ \left(\frac{\partial^2}{\partial x^2} + \frac{\partial^2}{\partial z^2} \right) \frac{\partial^2}{\partial t^2} + N^2 \frac{\partial^2}{\partial x^2} \right\} w_3 = \mathcal{L}\{w_3\} = \sum_i^2 \sum_j^2 \eta_1 (w_i w_j),$$

$$(4b.2)\qquad -g \frac{\partial^2}{\partial x^2} w_3 = \sum_i^2 \sum_j^2 \eta_2 (w_i w_j), \quad z = 0.$$

As in the previous chapter, the nonlinear terms in the surface boundary condition are transferred to the interior equation by a substitution $w_3 = w_3' + \tilde{w}$, where $\tilde{w}$ satisfies

$$-g \frac{\partial^2 \tilde{w}}{\partial x^2} = \sum_i \sum_j \eta_2, \quad z = 0,$$

$$\tilde{w} = 0, \quad z = -D.$$

The equations for w_3' become

$$(4b.3) \qquad \mathcal{L}\{w_3'\} = -\mathcal{L}\{\tilde{w}\} + \sum_i \sum_j \eta_{ij} \,,$$

$$(4b.4) \qquad w_3' = 0 \,, \quad z = 0, -D.$$

Note that $\mathcal{L}\{\tilde{w}\} \neq 0$ since $\tilde{w}$ is a forced wave.

Solutions of (4b.3) of the form

$$(4b.5) \qquad w_3' = a_3 \sigma_3 f_3(z) \cos \chi_3 x \cos(\sigma_3 t + \theta_3)$$

can be obtained with

$$(4b.6) \qquad \chi_3 = \frac{n\pi}{L} \,, \quad f_3(0) = f_3(-D) = 0,$$

if the amplitude a_3 and phase θ_3 are allowed to vary slowly with time. Substituting (4b.5) into (4b.3) and letting $\sigma_3 = \sigma_{03}(1+\delta)$, $\gamma_3^2 = \chi_3^2 \left(\frac{N^2}{\sigma_{03}^2} - 1 \right)$, one gets

$$(4b.7) \qquad 2(\gamma_3^2 + \chi_3^2)\sigma_3^2 \left\{ \left(\delta\sigma_3 + \frac{d\theta_3}{dt} \right) a_3 \cos(\sigma_3 t + \theta_3) + \frac{da_3}{dt} \sin(\sigma_3 t + \theta_3) \right\} f_3(z) \cos \chi_3 x = \text{r.h.s. (4b.3)}$$

To obtain (4b.7), $\delta << 1$ and (4a.23) have been used. This equation must be averaged to obtain the explicit equations for $\frac{da_3}{dt}$ and $\frac{d\theta_3}{dt}$. In order to do this a conjugate eigen function, $f_3^*(z)$,

must be introduced such that $\int_{-D}^{0} f(z) f^*(z)\, dz = 1$.

Thus,

$$(4b.8)\qquad a_3 \frac{d\theta_3}{dt} + \delta\sigma_3 q_3 =$$

$$\left(\frac{2}{L}\right)\left(\frac{\sigma_3}{\pi}\right) \frac{1}{2(\chi_3^2+\gamma_3^2)\sigma_3^2} \int_{-\pi/\sigma_3}^{\pi/\sigma_3} dt \int_0^L dx \int_{-D}^{0} dz \{\,\} \cos\chi_3 x \cos(\sigma_3 t+\theta_3)$$

$$(4b.9)\qquad \frac{dq_3}{dt} =$$

$$\left(\frac{2}{L}\right)\left(\frac{\sigma_3}{\pi}\right) \frac{1}{2(\gamma_3^2+\chi_3^2)\sigma_3^2} \int\int\int dx\, dt\, dz \{\,\} \cos\chi_3 x \sin(\sigma_3 t+\theta_3)$$

where

$$(4b.10)\qquad \{\,\} = \text{r.h.s. } (4b.3) \cdot f_3^*(z)$$

The solutions for which resonant growth is possible are those with $\chi_i \pm \chi_j - \chi_3 = 0$, $\sigma_i \pm \sigma_j - \sigma_3 = 0$. The strength of the interaction depends greatly upon

$$(4b.11)\qquad \text{the integral} \quad \int_{-D}^{0} f_3^*(z) \left[\sum_i \sum_j \mathcal{N}_1 - \mathcal{L}\{\tilde{w}\} \right] dz .$$

When the nonlinear forcing overlaps the vertical eigen function $f_3^*(z)$, the value of the integral will be large. Conversely, when the nonlinear forcing does not overlap $f_3^*(z)$, the interaction will be weak. The vertical dependence of $\Sigma\Sigma\eta_1$ and $\mathcal{L}\{\tilde{w}\}$ are not the same. Terms in η_1 are of the form $exp[(\chi_i+\chi_j)z]$. For high frequency surface waves, these decay rather quickly with depth. The forced wave $\tilde{w}$ has the following form:

$$(46.12) \qquad \tilde{w} = \frac{z+D}{gD}\sum_i^2\sum_j^2 \frac{\eta_2(\omega_i\omega_j)}{\hat{\chi}^2}, \quad \hat{\chi} = \chi_i \pm \chi_j .$$

It decays linearly with depth and has a better overlap with the low mode eigen functions $f_3^*(z)$. If the Brunt-Väisälä frequency N^2 is constant, then

$$(46.13) \qquad f^*(z) = \frac{2}{D}\sin\frac{m\pi}{D}(z+D), \quad m = 1, 2, \cdots,$$

and the integral (46.11) may be evaluated. The phase and amplitude equations, (46.8) and (46.9) then reduce to

$$(46.14) \qquad a_3\frac{d\theta_3}{dt} + \delta\sigma_3 a_3 = I\sin(\theta_1+\theta_2-\theta_3)$$

$$(46.15) \qquad \frac{da_3}{dt} = I\cos(\theta_1+\theta_2-\theta_3)$$

where

$$(46.16)\qquad I = \frac{(-1)^{m+1}\, m\pi N \chi_3 D}{\left[(\chi_3 D)^2 + (m\pi)^2\right]^{3/2}} \frac{a_1 a_2 \sigma_1 \sigma_2}{g} \begin{cases} 1 - 4 \dfrac{(\chi_3 D)^2 + (m\pi)^2}{(\chi_1+\chi_2)^2 D^2 + (m\pi)^2}, & \delta = -1, \\ -3, & \delta = +1, \end{cases}$$

and $\chi_3 = \chi_1 + \delta \chi_2$, $\sigma_3 = \sigma_1 - \sigma_2$.

Note that both $\chi_1 - \chi_2$ and $\chi_1 + \chi_2$ can simultaneously satisfy $N^2 \chi_3^2 \left[\chi_3^2 + \left(\frac{m\pi}{D}\right)^2\right]^{-1} = \sigma_{03}^2$. If $\chi_1 = \frac{n_1 \pi}{L}$, $\chi_2 = \frac{n_2 \pi}{L}$ then $\chi_1 - \chi_2 = (n_1 - n_2)\frac{\pi}{L}$ and $\chi_1 + \chi_2 = (n_1 + n_2)\frac{\pi}{L}$. The vertical mode number m will be different in each case. The growth rate for the higher modes ($\delta = +1$) is much less, however, than for the lower modes. Thus with $\delta = -1$, (46.16) becomes

$$(46.17)\qquad I = \frac{(-1)^{m+1}\, m\pi N \chi_3 D}{\left[(\chi_3 D)^2 + (m\pi)^2\right]^{3/2}} \frac{a_1 a_2 \sigma_1 \sigma_2}{g} \left\{ 1 - 4 \frac{(\chi_3 D)^2 + (m\pi)^2}{(\chi_1+\chi_2)^2 D^2 + (m\pi)^2} \right\}$$

Note that for $\chi_1, \chi_2 \gg \chi_3$, the second term in (46.17) becomes unimportant. This term arises from the original nonlinear terms in the interior equation (46.1), while the first term represents the nonlinear terms in the free surface boundary condition (46.2). As was the case

with the two-layer model in Chapter III, the direct action of the surface waves upon the internal wave is negligible compared to the indirect action through the surface boundary condition. Thorpe's result (1966-A) for a constant N^2 model and progressive waves closely resembles equation (46.17). Thorpe found

$$(46.18) \qquad I = \frac{m\pi N \chi_3 D}{2\left[(\chi_3 D)^2+(m\pi)^2\right]^{3/2}} \frac{a_1 a_2 \sigma_1 \sigma_2}{g} [\ ]$$

where

$$(46.19) \qquad [\ ] = 3+2\cos\alpha+(-1)^{m+1}3(1+\cos\alpha)\frac{(\chi_3 D)^2+(m\pi)^2}{(\chi_1+\chi_2)^2 D^2+(m\pi)^2},$$

$$\cos\alpha = \frac{\vec{\chi}_1 \cdot \vec{\chi}_2}{\chi_1 \chi_2}$$

C. Modification due to viscosity

We now introduce a viscous decay coefficient for the internal wave. The primary source of viscous dissipation for the parameter range considered in the laboratory experiment is due to thin side wall boundary layers. The decay factor can be found both experimentally and theoretically and the results compared. The theoretical result is presented in the appendix. In this section, the decay factor λ will be a known

constant for each mode. The resonance equations (4b.11) and (4b.15) become

$$a_3 \frac{d\theta_3}{dt} + \delta\sigma_3 a_3 = I \sin(\theta+\pi), \tag{4b.20}$$

$$\theta \equiv \theta_3 - \theta_1 + \theta_2,$$

$$\frac{da_3}{dt} + \lambda_3 a_3 = -I\cos(\theta+\pi). \tag{4b.21}$$

These equations were solved in the previous chapter under the assumption that the interaction term, I, was constant. Under this same constraint, the previous solutions may be used for these equations with I given instead by (4b.17).

CHAPTER V. Results and Discussion

The data and the predictions from Chapters III and IV will be presented for three basic experiments (4,5,6); experiments 4 and 5 had steplike density profiles, experiment 6 a linear one.

Profiles of N^2 are shown in Figure V-1. The interface in experiment 4 was placed successively at z =-50 cm(4a), -40 cm (4b), and -30 cm(4c). The latter case is shown in Figure V-1. Results from each experiment will be presented separately except for Table 1 which lists most of the relevant parameters for all three, (see appendix).

A. Two layer experiments

In experiment 4, the fundamental internal wave (n=1) was selected for the third member of a resonant triad. Steady state amplitude responses obtained from the pressure transducer and particle motion are shown for each of three interface depths in Figure V-2. The intensification of the response as the interface was raised from 50 cm (●) to 40 cm (◐) (two surface wavelengths) from the free surface is apparent. The theoretical curve for interface depth of 30 cm predicts a greater intensification near the resonance peak than was evident. Away from the maximum, however, the agreement is quite good. The phase response for this experiment (4c) is shown in Figure V-3. Phases were computed by cross-correlating the pressure signal with the resolver reference signal. Except for the case of no detuning, all phases were underpredicted. This was partly a result of the correlation technique which averaged over phases that were, in many cases,

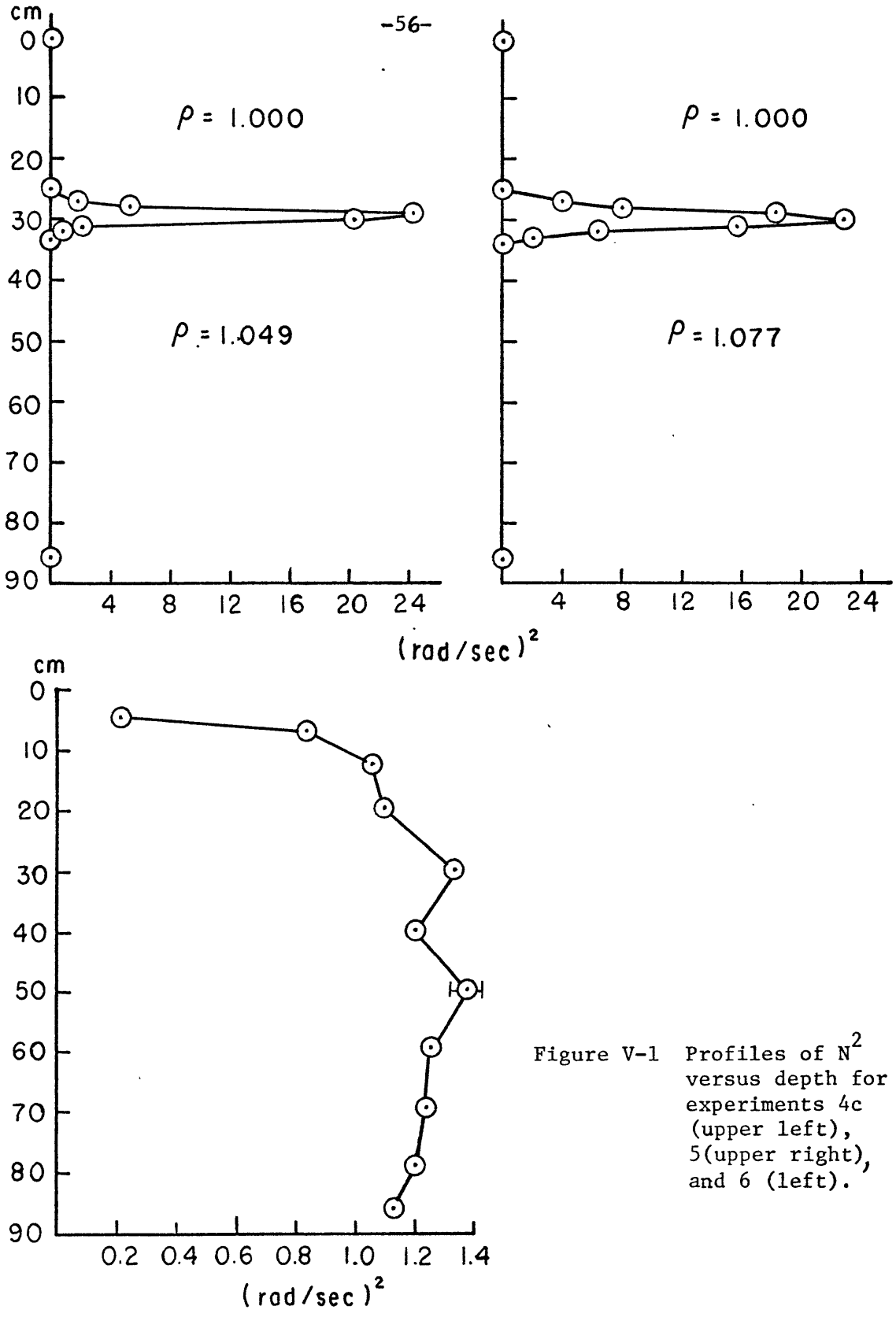

Figure V-1 Profiles of N^2 versus depth for experiments 4c (upper left), 5(upper right), and 6 (left).

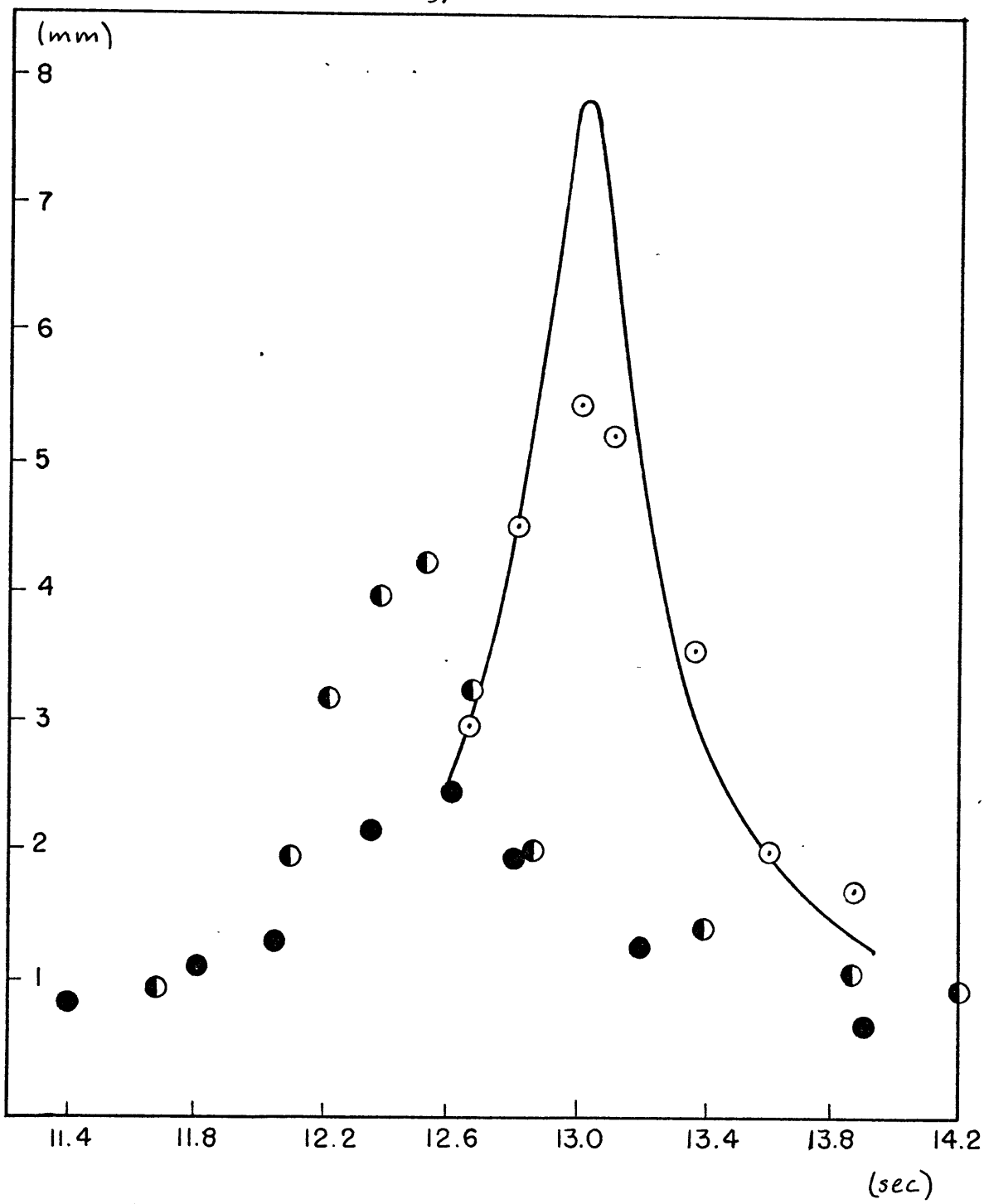

Figure V-2 Internal wave amplitude response for experiment 4 with interface depth of 50cm (●), 40 (◐), and 30 (⊙).

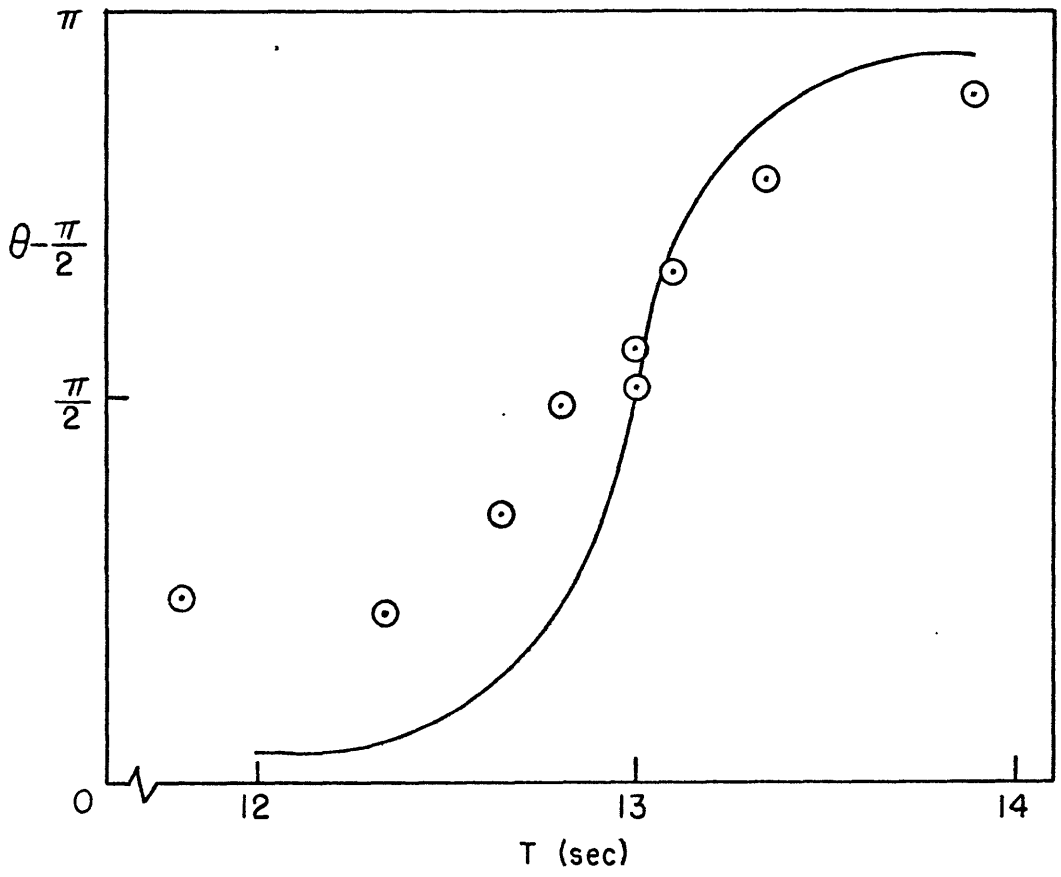

Figure V-3 Phase response of internal wave for experiment 4c

still increasing away from $\pi/2$. All theoretical steady state predictions depend strongly upon the internal wave dissipation parameter, λ. This quantity was measured independently from resonant interaction effects by turning <u>both</u> motors off and observing the decay of a resonantly excited wave. Shown in Figure V-4 is the decay of the free mode (T = 12.98 sec.) internal wave. The theoretical decay rate is slightly less than the least squares result. The observed value was used in preference to the theoretical one.

The growth to steady state of the tuned internal wave is shown in Figure V-5. When the wave reached 90% of its final value (5.5 mm), the observed growth suddenly decreased from the predicted, viscously limited curve. The resonant growth of a detuned wave is presented in Figure V-6. A small constant offset between theory and experiment is apparent in this figure. Both cases are presented on Plate V-1, which shows the strip chart recordings made during both runs. The surface wave amplitude, $a(t)$, is the third trace in each set. It can be seen (in the lower set) that a distortion in the surface wave field develops for the tuned case after several internal wave periods. This distortion was present in some form for tuned resonance in all experiments. Further discussion of this effect will be found in a later section. The temporal variation of phase $\Theta \equiv \Theta_3 - \Theta_1 + \Theta_2$ for the detuned and tuned cases are shown in Figures V-7 and 8. For the detuned case, the measured and predicted phase and an amplitude (see Figure V-6) differ by a constant offset. These two discrepancies are theoretically

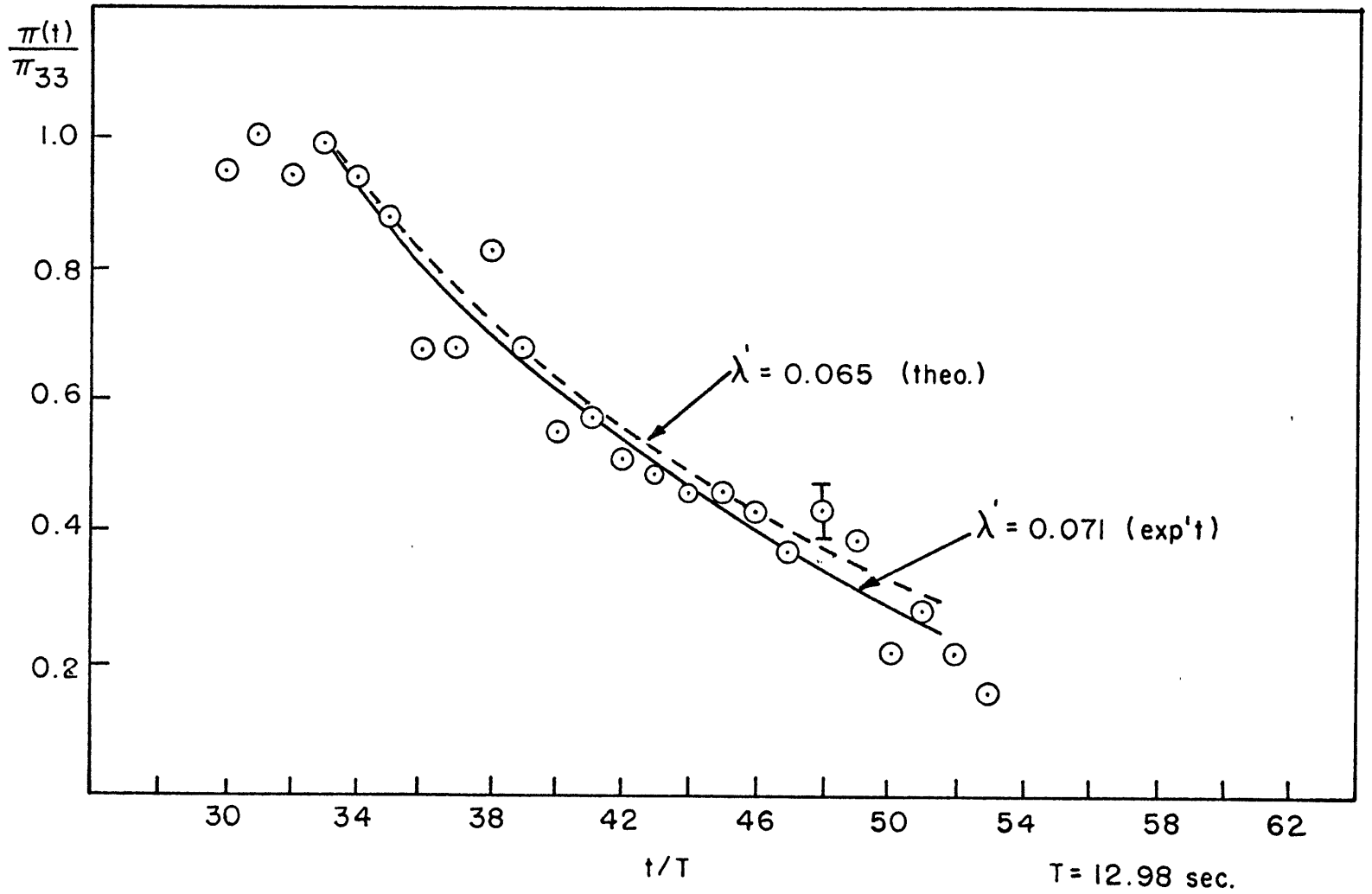

Figure V-4 Viscous decay of free mode internal wave for experiment 4c, $\lambda' = \frac{2\pi}{\sqrt{3}} \lambda_3$.

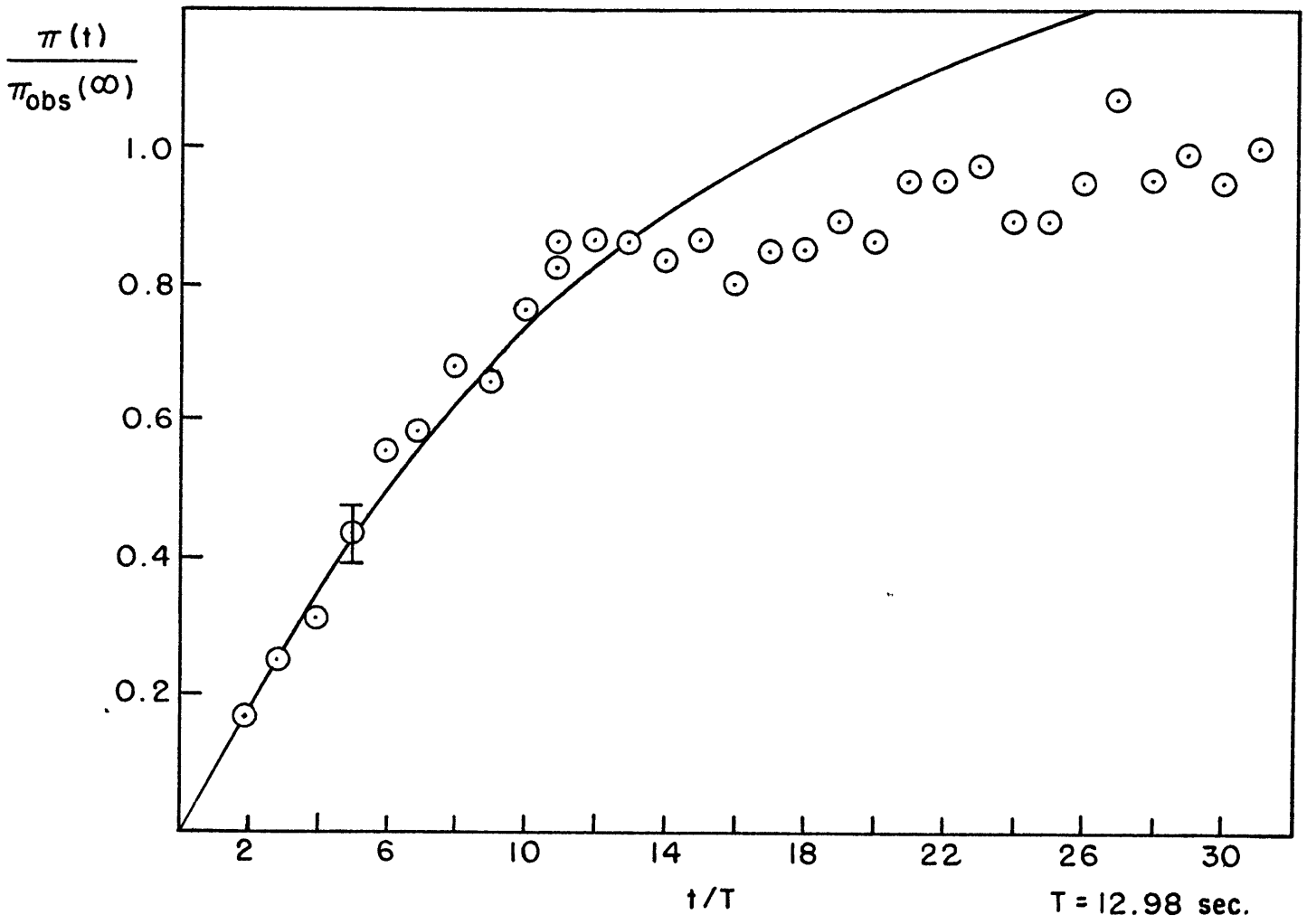

Figure V-5 Resonant growth of tuned internal wave for experiment 4c

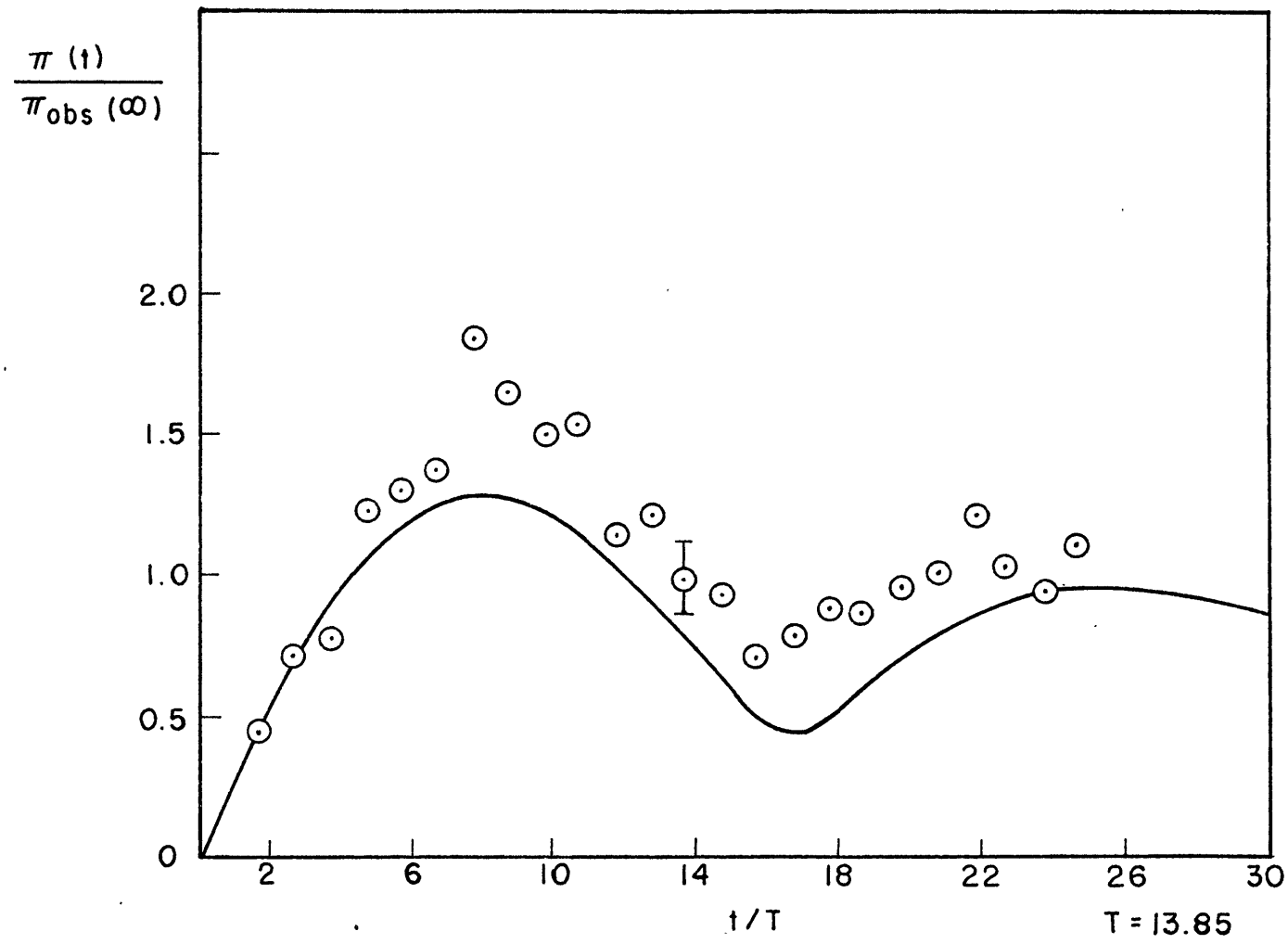

Figure V-6 Resonant growth of detuned (δ=.061) internal wave for experiment 4c

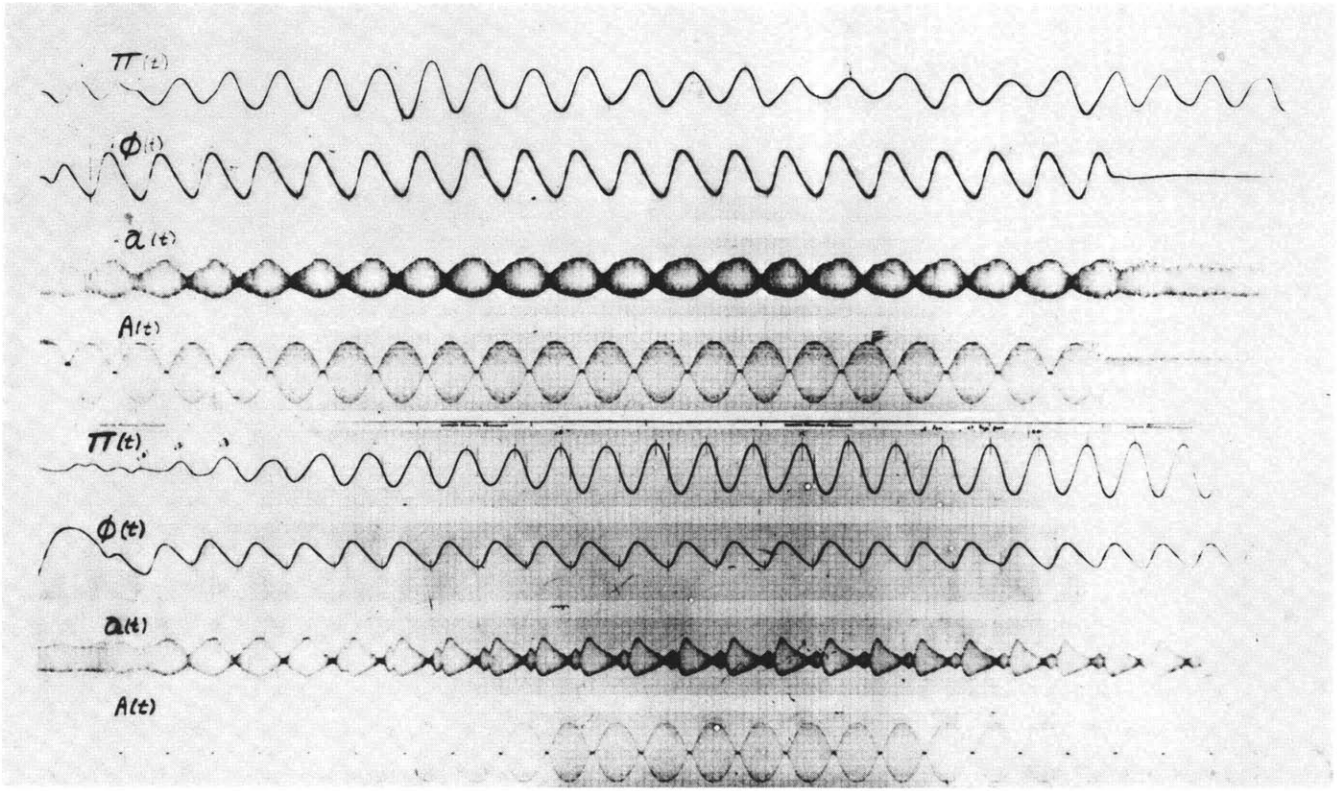

Plate V-1

Experiment #4c $\Delta\rho$ =0.049, n=1

Growth of detuned wave (δ =0.061): top 4 traces.

Growth of tuned wave (T= 12.98 sec): bottom 4 traces.

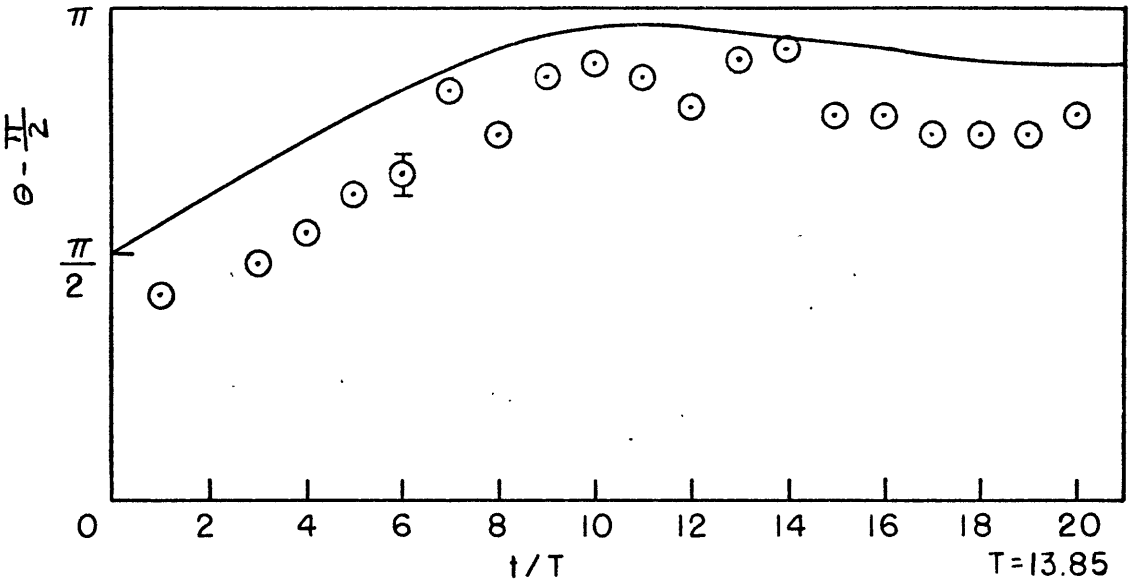

Figure V-7 Phase of detuned (δ=.061) internal wave for experiment 4c

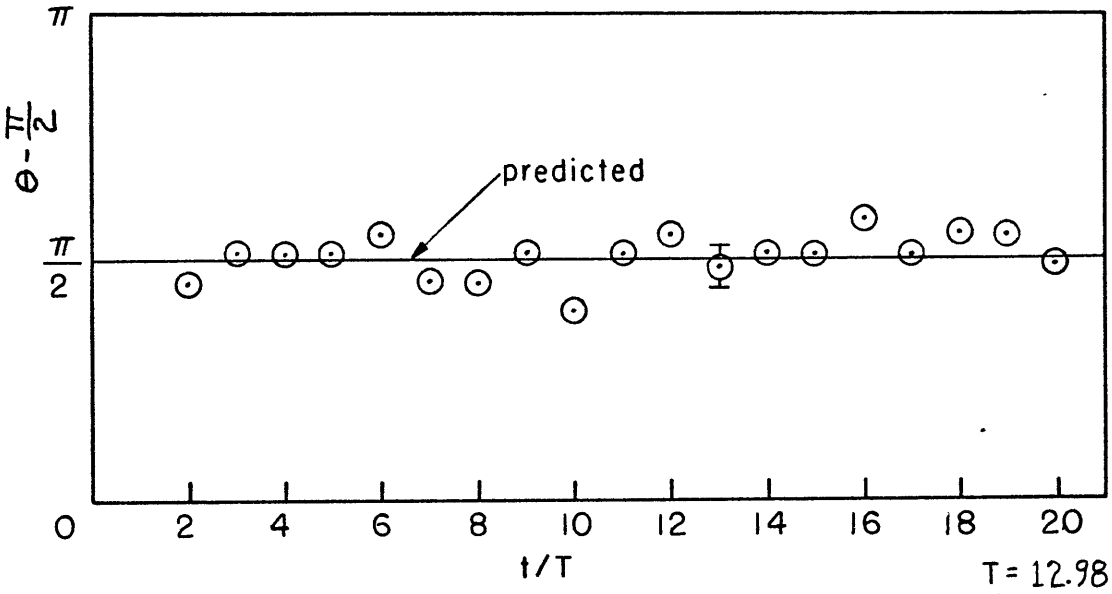

Figure V-8 Phase of tuned internal wave for experiment 4c

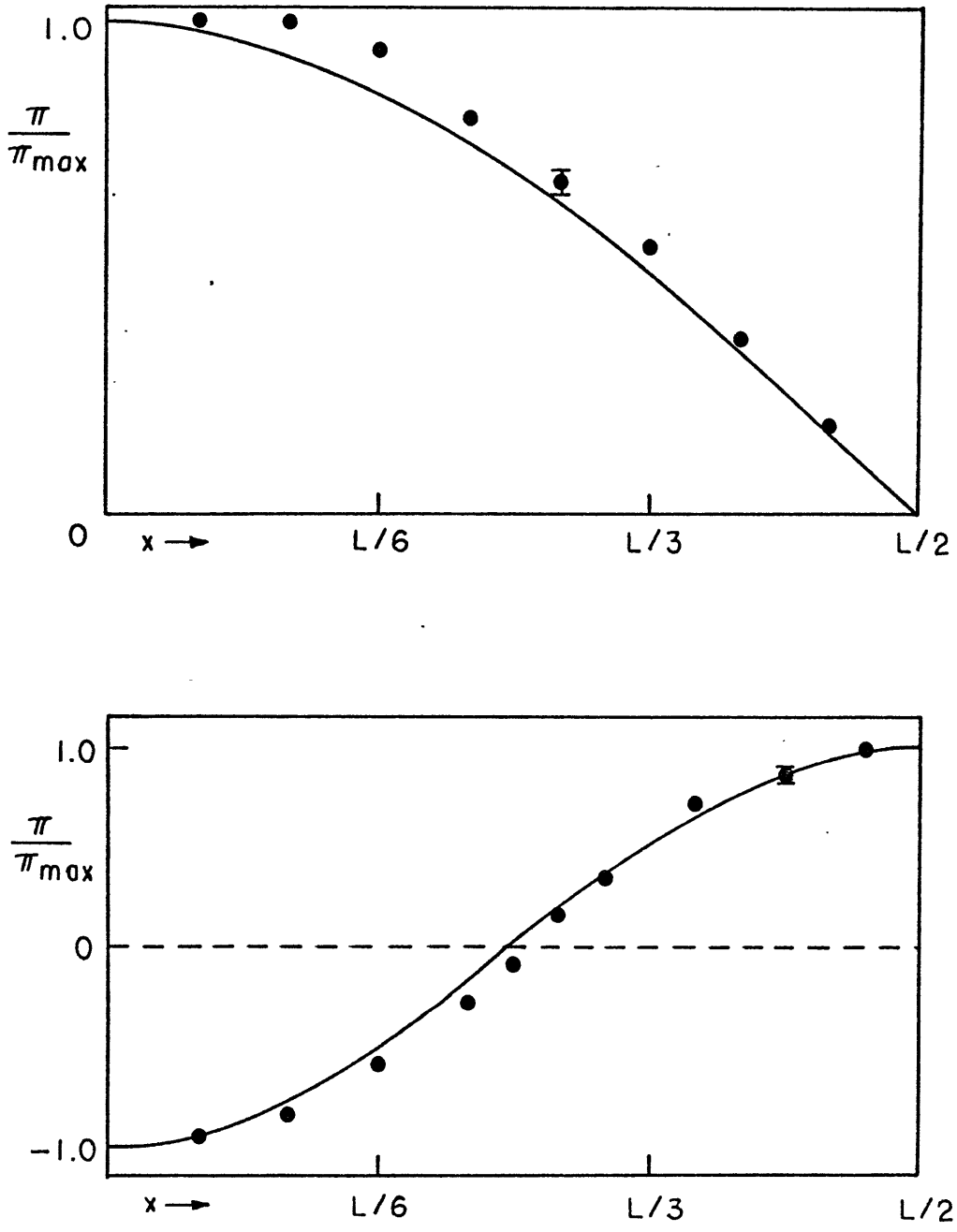

Figure V-9 Dependence of pressure upon horizontal position for the tuned n=1 (upper) and n=2 (lower) internal wave at a depth Z=-13 cm., L = 2D = 180 cm.

related however; an over predicted phase will result in an under-predicted amplitude of the resonant detuned internal wave. For the tuned case in Figure V-8, agreement with theory is within the experimental error of phase determination. The dependence of pressure on horizontal position is given in Figure V-9 for the tuned case. Also shown is the dependence of the second horizontal ($n = 2$) mode internal wave of experiment 5. Other results for experiment 5 are shown in Figures V-10, 11.

The steady-state amplitude response of the internal wave for different surface wave forcing periods is shown in Figure V-10. The tuned, resonant growth of the 6.08 sec wave presented in Figure V-11 shows a close agreement between predicted and observed interface amplitude. The surface wave profile during this interaction experiment showed little visible distortion, yet in fact a surface amplitude spectrum indicated otherwise. This will be discussed in section C.

B. Linear stratification

The interaction theory developed in Chapter IV was tested for a linear stratification (see Figure V-1) in experiment 6. Only the first vertical and first horizontal mode internal wave could be easily studied. Higher forced modes could be generated with large amounts of detuning, but the free modes required excessive amounts of salt for tuning.

The pressure amplitude response in terms of maximum vertical particle excursion is shown in Figure V-12. For small detu ning, measured amplitudes are smaller than predicted. Otherwise the agreement

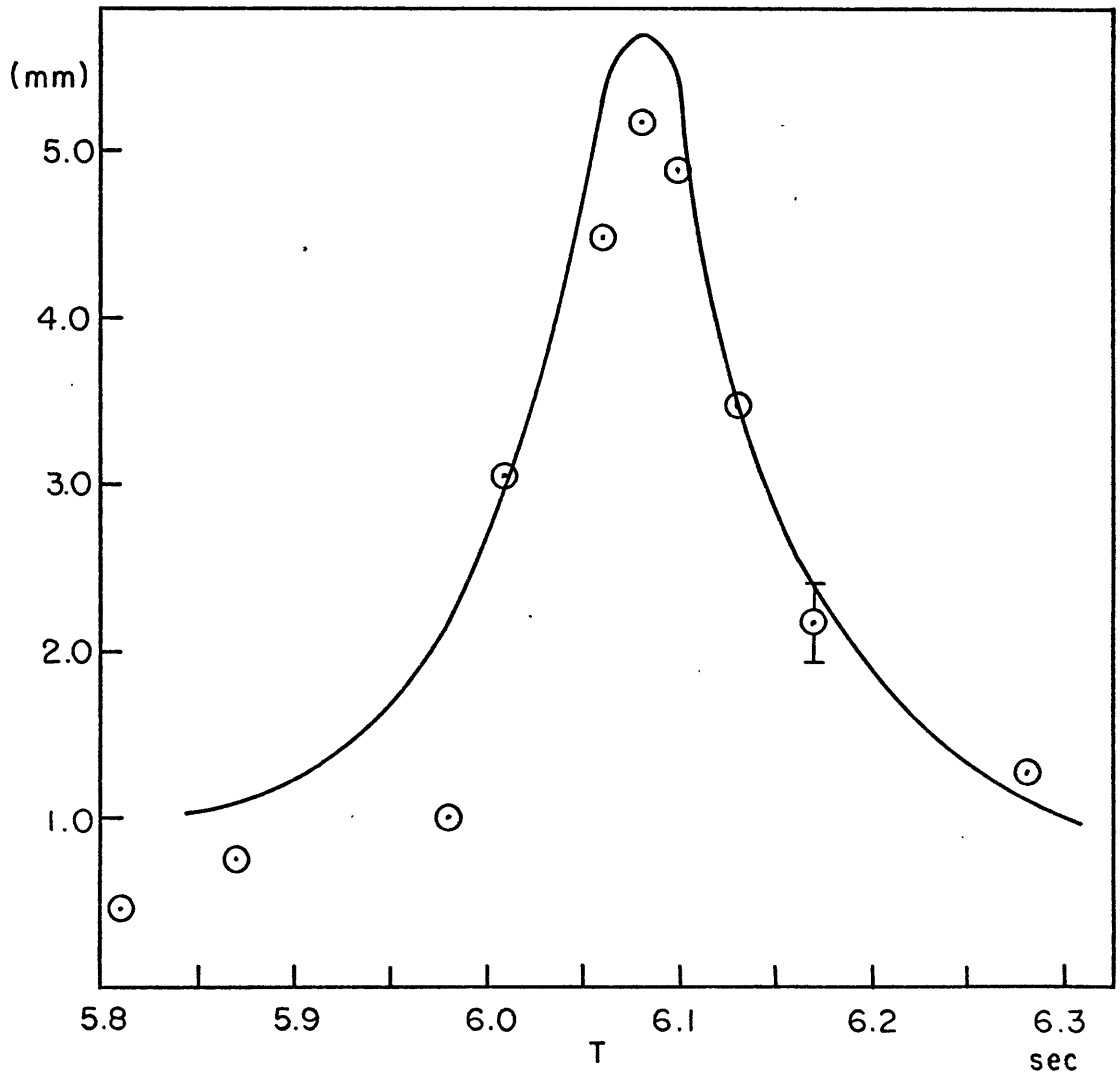

Figure V-10 Second horizontal mode (n=2) internal wave amplitude response for experiment 5

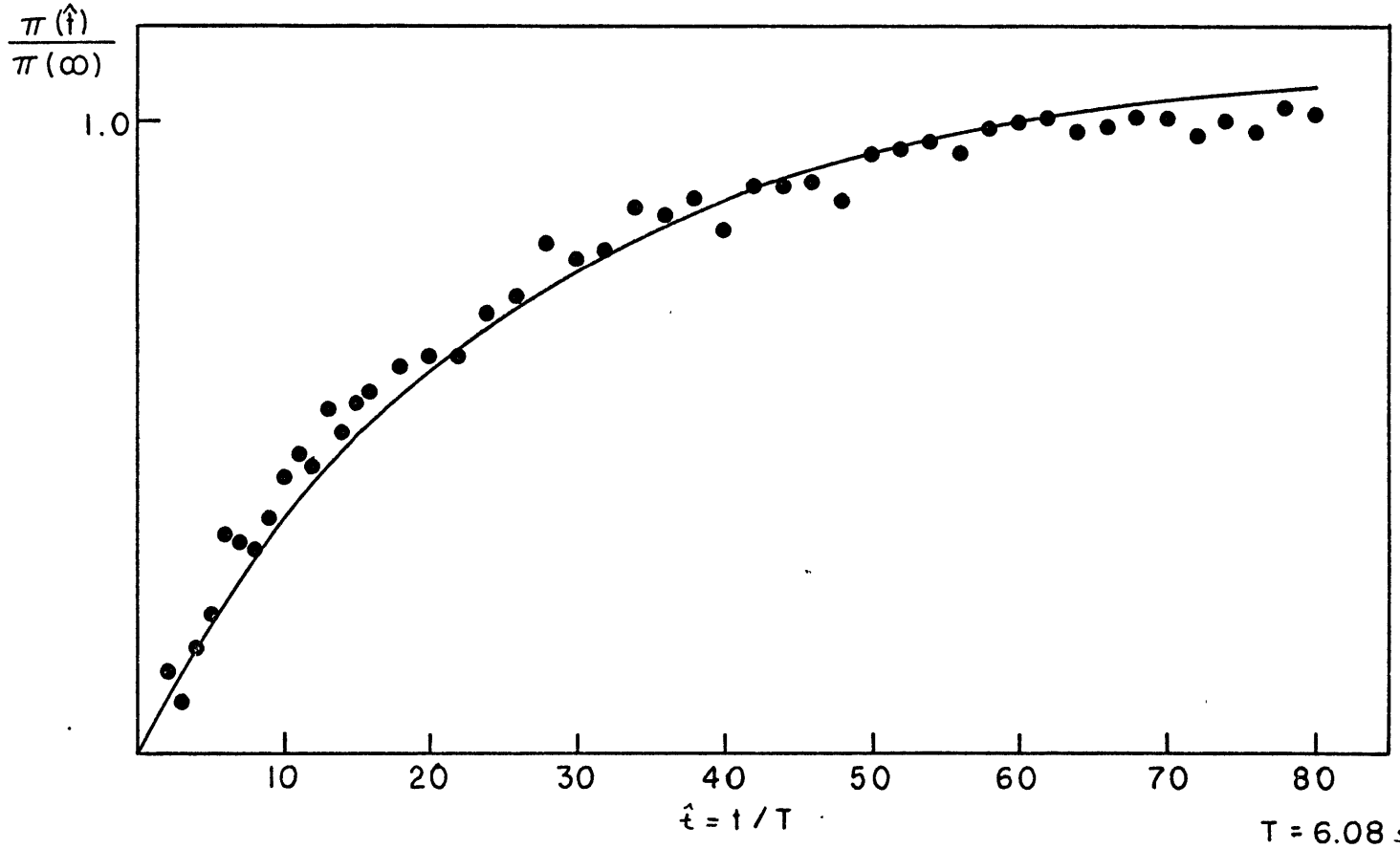

Figure V-11 Resonant growth of a tuned second mode internal wave for experiment 5

with theory is quite good. The observed amplitude growth for $\delta = 0.0$ and .056 is plotted in Figure V-13 along with the predicted curve for $\delta = 0$. The predicted growth rate is smaller and the final amplitude larger than the observed amplitudes for the tuned ($\delta = 0$) case. The former effect is due in part to the fact that the forced surface wave contributes to the measured pressue by an amount equal to approximately 1/7 the measured pressure after two internal wave periods. Thus the actual pressure due to the internal wave is the measured value less the forced wave value <u>if</u> the two pressures are in phase, which is the case for small detuning. This effect is present in all three experiments 4c, 5, and 6. The small offset is independent of time and the frequency of the internal wave but dependent upon the phase of the internal wave relative to the forced surface wave. Figure V-14 indicates a phase determination by the crosscorrelation technique. The resolver output was crosscorrelated with the pressure probe output $\pi(t)$ which is the actual pressure $p(t)$ shifted 180° in phase, or electrically inverted. Note that the measured pressure leads the reference signal by approximately 90° instead of lagging by 90° as was the case for experiments 4 and 5. This result is predicted by the theory (compare 3c4 and 4b21). Physically, however, the vertical velocity of the internal wave near the free surface is in phase with the vertical velocity of the forced surface wave for $\delta = 0$ in all cases.

The experimental decay parameter λ, was determined in two different ways. In Figure V-15, the solid line and circles represent the decay of the $n=1, m=1$ mode internal wave when both motors were stopped.

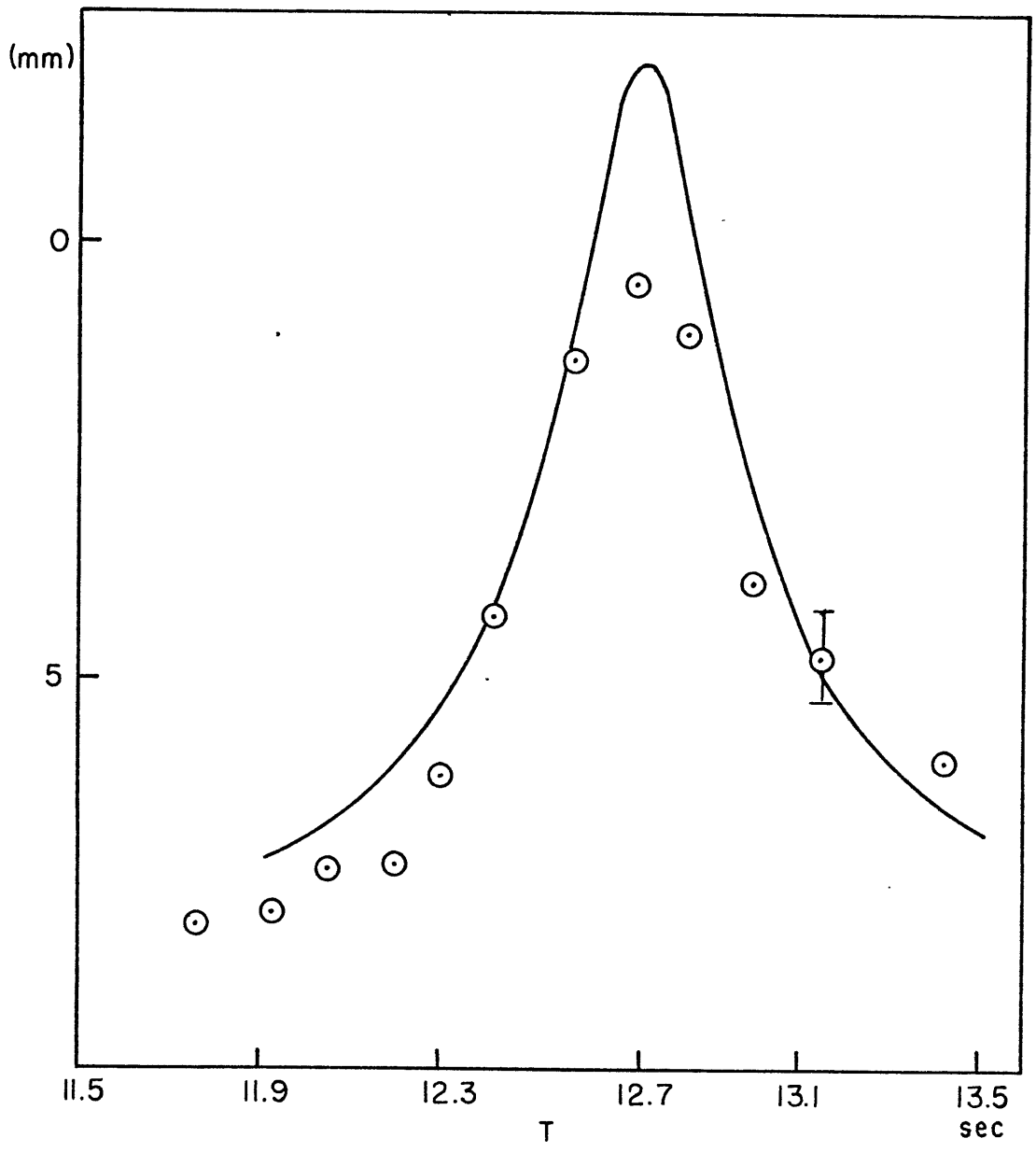

Figure V-12 Amplitude response of n=1, m=1 internal wave for a constant N stratification for experiment 6

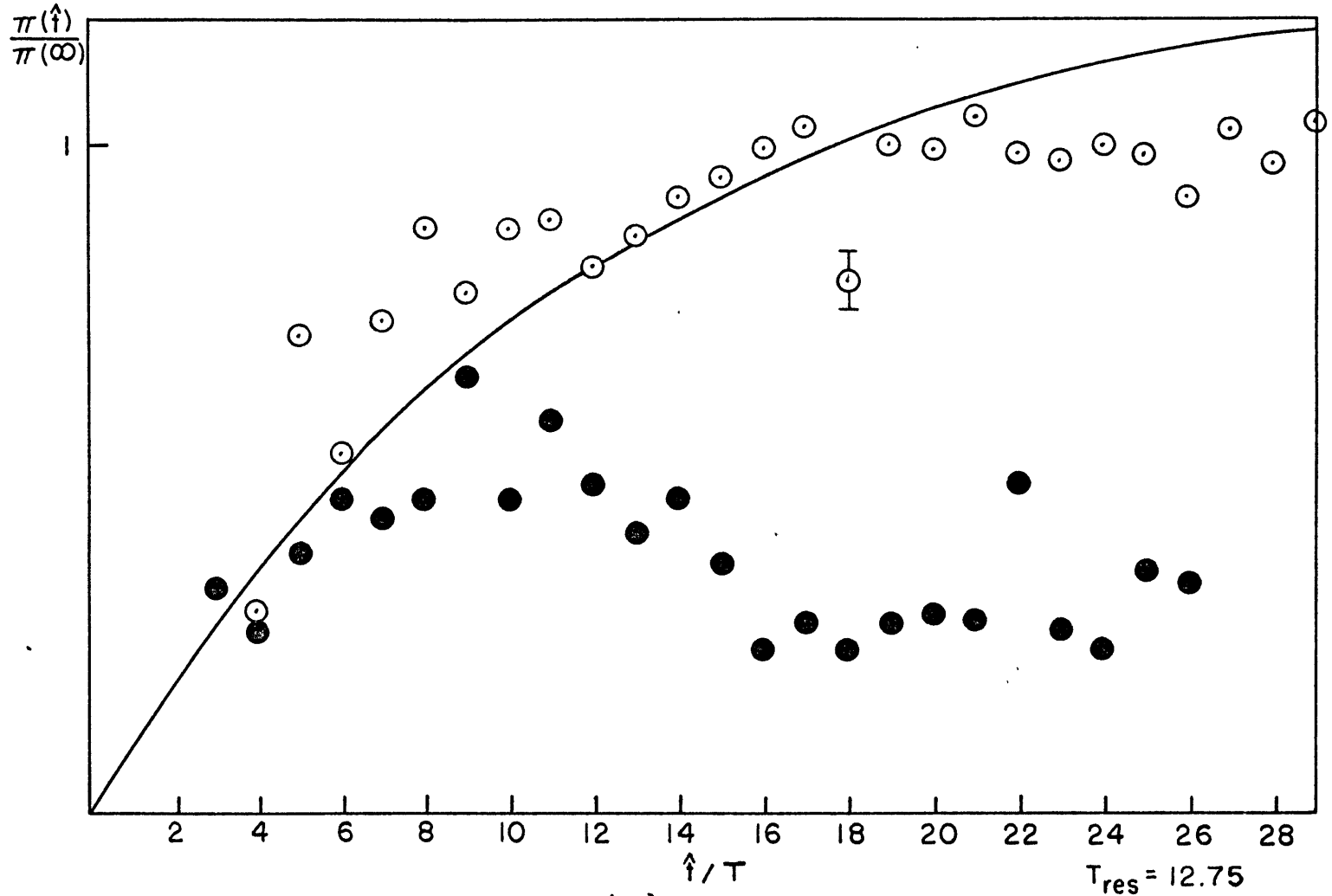

Figure V-13 Growth rates for tuned (⊙) and detuned ($\delta = 0.056$) n=1, m=1 internal wave for experiment 6

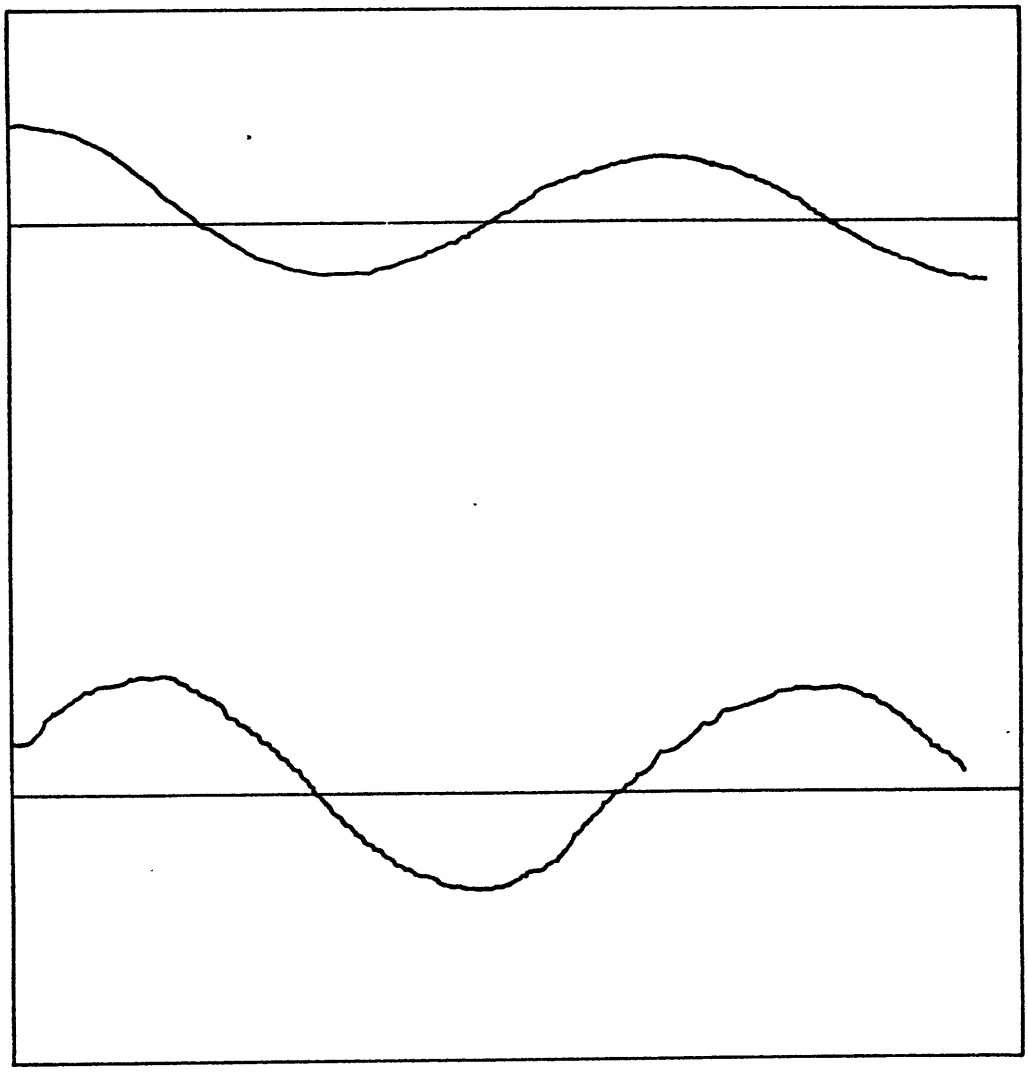

Figure V-14 Phase determination by crosscorrelation technique for experiment 6. Top trace: auto correlation, $R(\phi(t)\,\phi(t+\tau))$ versus τ. Bottom trace: cross correlation $R(\pi/4)\,\phi(t+\tau))$ versus τ.

With one motor off, the decay of the internal wave follows the dashed line and open circles. In the former case, the internal wave decays in the absence of any surface waves. In the latter case, however, one surface wave is present and interacts with the decaying internal wave to generate another surface wave. The internal wave loses energy to viscosity and to a surface wave through a nonlinear interaction. This effect was documented in experiment 5. When one of the motors was turned off, a modulation in the surface wave profile continued for over 20 internal wave periods (300 surface wave periods). The decrease in modulation followed closely the decay of the tuned internal wave.

The dependence of pressure on horizontal position and depth is shown in Figure V-16. Plotted also are the predicted cosine curves for the constant N stratification.

C. Discussion

Evident in all three experiments presented is that the nearly tuned, steady-state internal wave amplitude is smaller than predicted by the theory of chapters III and IV. Experimental errors in the determination of viscous decay parameters and initial growth rates used in the theoretical predictions are of order 10% at worst (usually only 5%). Plate V-1 indicated that the surface wave field became distorted during the growth of a tuned internal wave. Clearly, the assumption that the surface wave field remains unaffected during the interaction is not always valid. The back interaction process

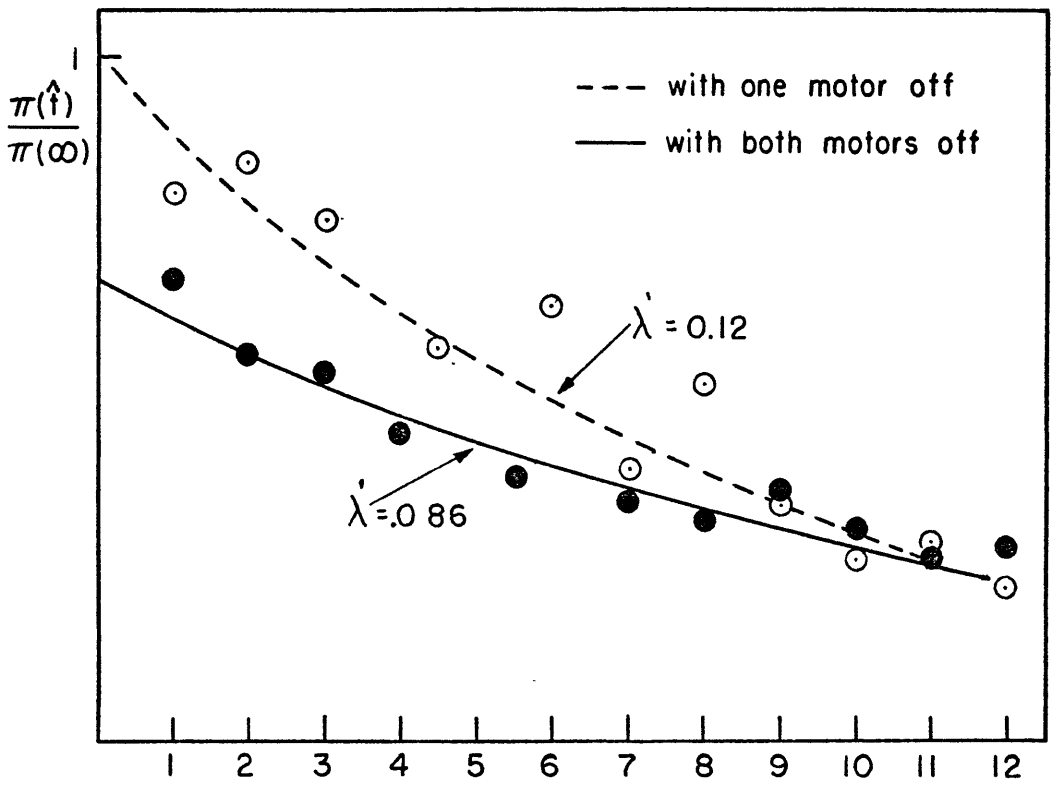

Figure V-15 The effect of the nonlinear interaction upon the decay of the free n=1, m=1 mode for a constant N stratification for experiment 6, $\lambda' = \frac{2\pi}{\sqrt{3}} \lambda_3$.

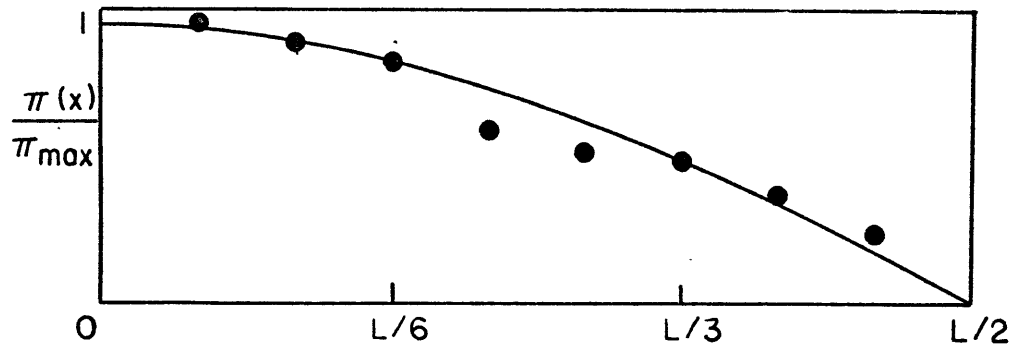

Figure V-16 Pressure dependence with horizontal position (upper) for Z =-13 cm and with depth (lower) for x =20 cm (experiment 6), L= 2D = 180 cm.

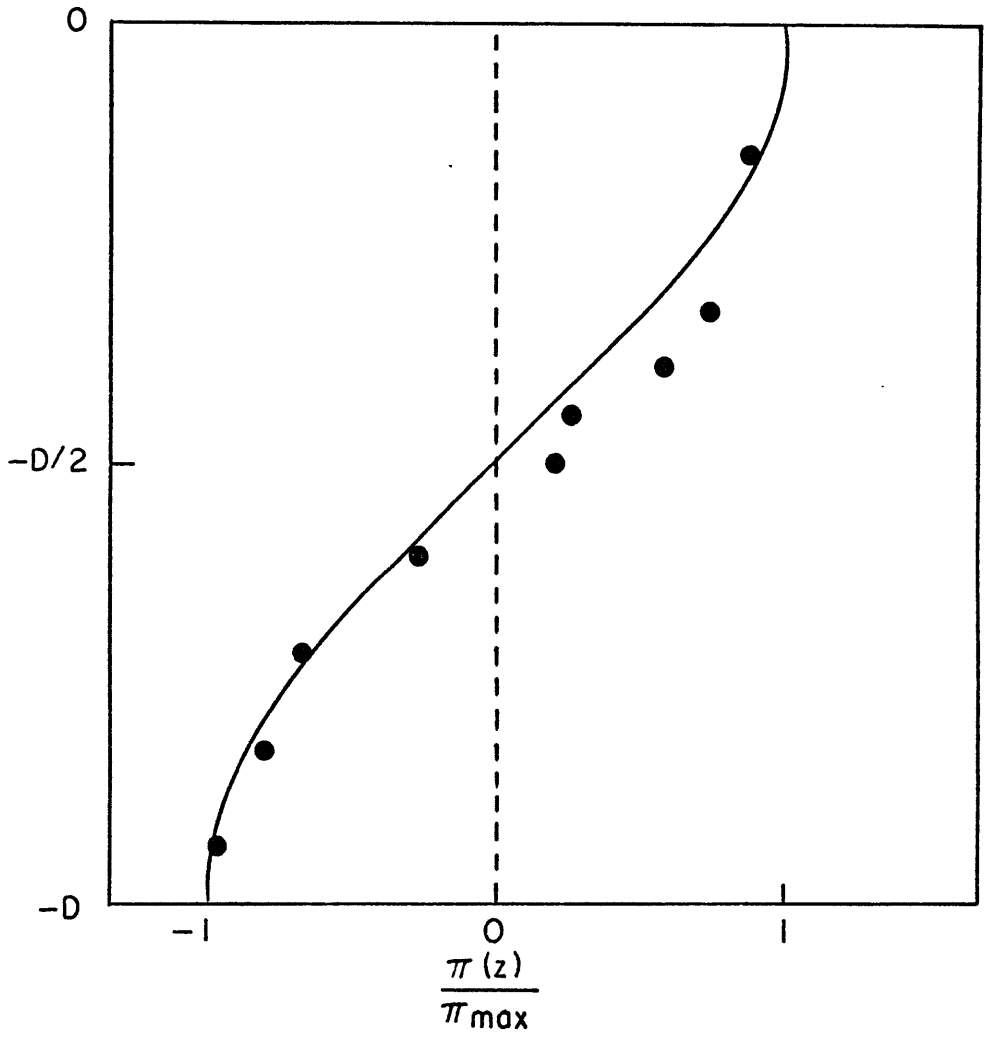

in the experiments performed is not as simple as might first be expected. The inviscid, unforced equations for a single triad of interacting waves, two surface and one internal, are discussed in the theoretical appendix. The system of three waves is not closed, however. For surface eigen frequencies used in the experiments, the separation in frequency between pairs of adjacent peaks is nearly uniform. For example, if a mode #20 and a mode #21 surface waves have a difference frequency equal to the natural frequency of a horizontal mode #1 internal wave, a resonant transfer of energy is possible to the internal wave. Since the difference frequency between modes #19 and #20 is 'almost' resonant, the internal wave and surface wave #20 can interact to produce a slightly detuned #19 mode. Amplitude spectra of the surface elevation indicate that the appearance of distortion is associated with the presence of as many as three additional surface waves.

Surface wave amplitude spectra were computed using the PAR correlator and fourier analyzer with tape loops containing approximately 400 surface waves (20 internal wave periods). The record length for computation of 35 surface waves was chosen so as to be long enough to resolve two frequencies differing by 6% (16 surface waves) yet short enough to prevent aliasing (50 surface waves). The spectra shown in Figures V-17, 18 represent averages over the record length of 20 internal wave periods. The change in the spectrum with time is indicated by successive surface wave spectra. The paddle motion is included for reference.

The spectra of Figure V-17 for the tuned internal wave of Figure V-11 clearly show a loss of energy of the higher paddle forced surface wave and a gain of energy of a third surface wave of lower frequency

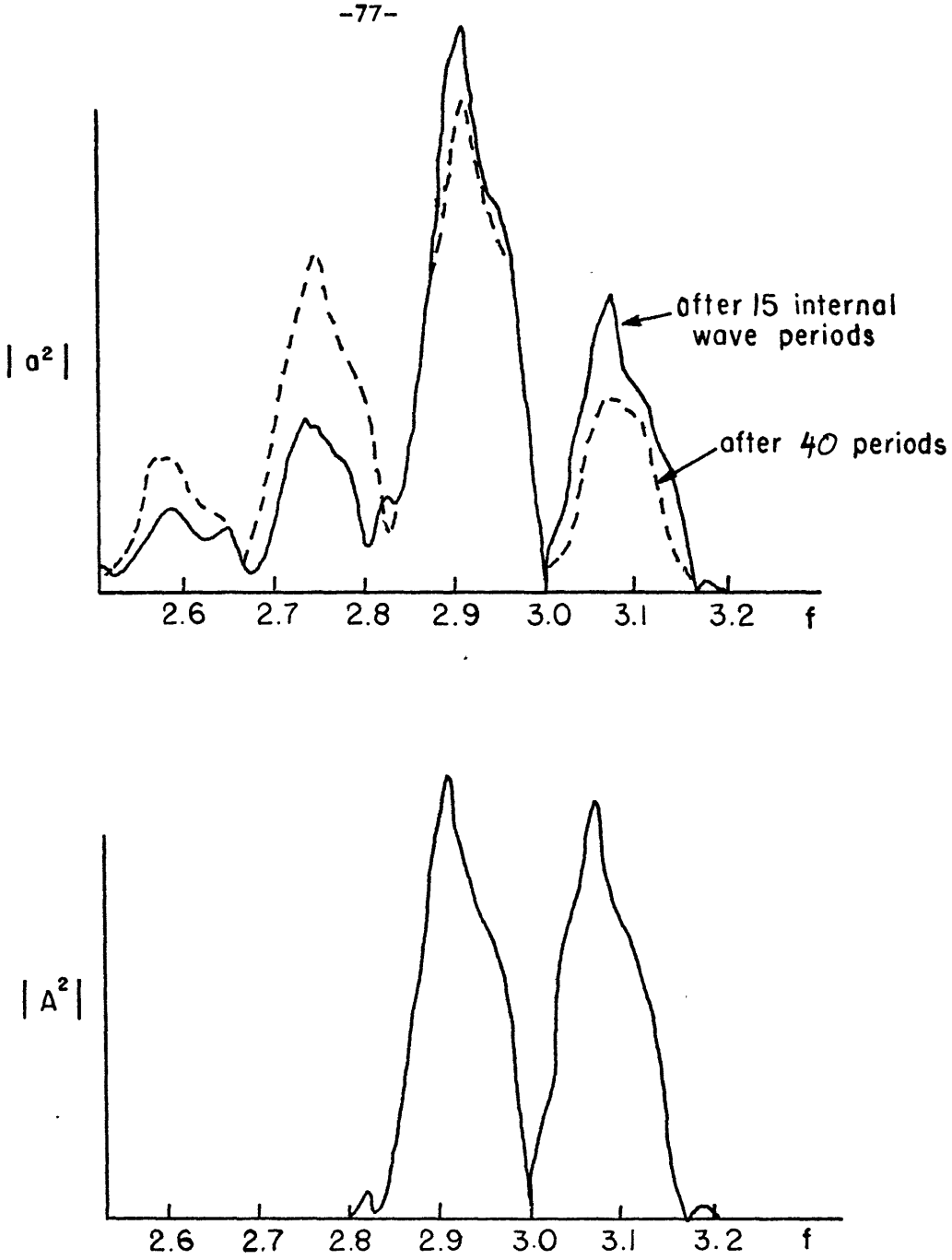

Figure V-17 Amplitude spectra versus frequency (hz) for surface waves (upper) and paddle (lower) in experiment 5 (δ =0)

which, being unforced by the paddle, was initially absent. Other "lumps" at higher and lower frequencies appear, but these remain small. The new surface wave at f = 2.65 Hz eventually becomes as large as the initial paddle forced wave! The rate of change of the spectrum becomes less after 50 internal wave periods. It is not clear, however, that an asymptotic state had been reached before one of the motors was turned off (at t/T = 80) causing a decay of the internal wave and all but one of the surface waves. Figures V-11, 17 together provide a complete picture of the important waves involved in this example. What is somewhat baffling is the good agreement between the experiment and a theory which assumes no change in the surface wave spectrum.

A detuned internal wave of period 6.28 sec was generated in experiment 5 having an amplitude as shown in Figure V-10 which was predicted to within the experimental error of the measurement. The surface wave spectrum of Figure V-18 shows no significant change throughout the growth to steady-state of the detuned, resonant internal wave.

The general features of experiment 5 are common to all experiments performed. As the amount of detuning was decreased (with a corresponding increase in the amplitude of the internal wave), the number and amplitudes of identifiable new surface waves increased with a preference toward lower discreet frequencies. One theoretical and two experimental results suggest that the extra surface waves are generated by a nonlinear interaction between at least one existing surface wave and the resonantly growing internal wave. The experimental evidence is (1) the new surface waves appear when the internal wave amplitude is larger and (2) all sur-

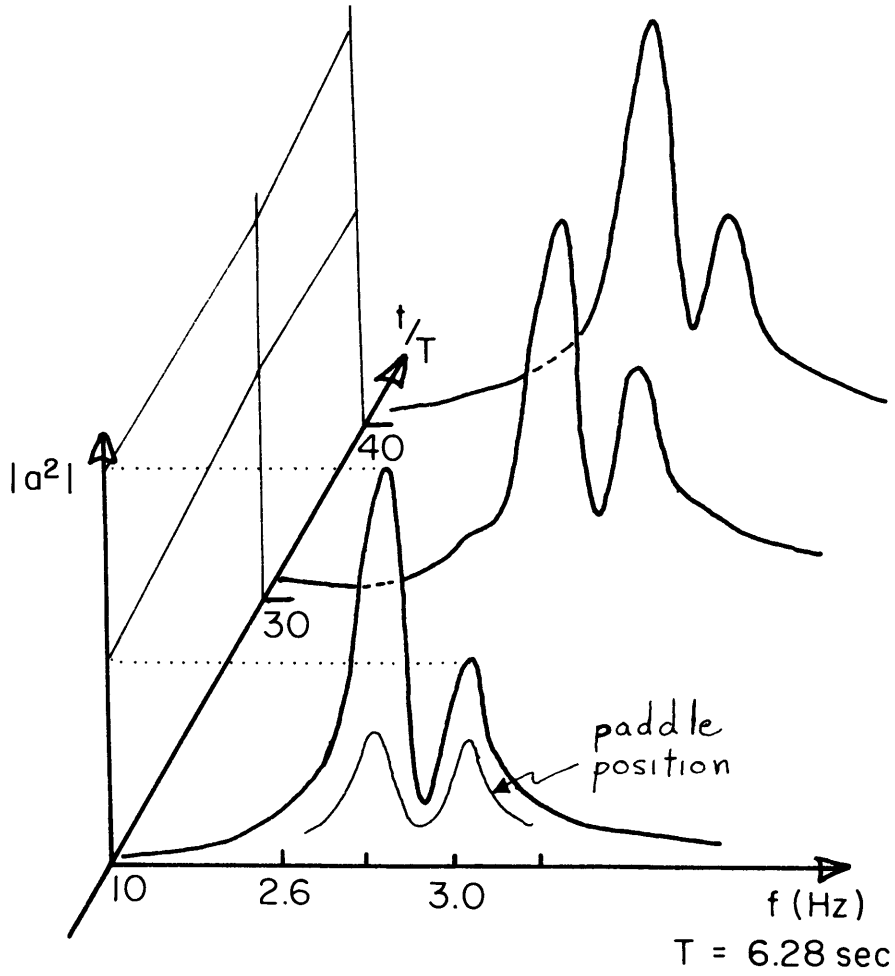

Figure V-18. Development of surface wave amplitude spectrum (at x = 0) vs. nondimensionalized time during resonant growth of a horizontal mode #2, detuned (δ = .033) internal wave of experiment 5. Successive spectra represent averages over 400 surface wave periods.

face waves (initial and new) have frequencies and wave numbers which always satisfy

$$\sigma_{isurf.} - \sigma_{jsurf.} = \sigma_{int} ,$$

$$\kappa_{isurf} - \kappa_{jsurf} = \kappa_{int} , \quad \kappa = \frac{n\pi}{L} , \quad n = 1, 2, \ldots .$$

In experiment 5, for example, only every <u>other</u> surface wave in the standing wave response curve can satisfy the second requirement since $\kappa_{int} = 2\pi/L$, and these are the only extra peaks to appear in Figure V-17. Intermediate peaks, if present, could have been resolved with the tape loop technique. The theoretical evidence arises from the nature of the interaction coefficient (see theoretical appendix) for the initial triad consisting of two surface waves (a_1, θ_1), (a_2, θ_2) and one internal wave (a_3, θ_3). It can be shown that the interaction coefficient for the growing internal wave is positive, while those for the surface waves of higher (a_1, θ_1) and lower (a_2, θ_2) frequencies are larger and of negative and positive sign respectively. This result is consistent with the stability criterion of Hasselmann (1967). Hence the surface wave of higher frequency loses energy to the internal wave and the other surface wave. This surface wave and the growing internal wave can in turn generate a nearly tuned third surface wave as described earlier. Thus, a preferential direction toward lower frequencies should be expected. This effect is in fact observed. It is instructive to note that if the phase of the new surface wave (a_4, θ_4) is equal to that of the wave it is replacing (a_1, θ_1), the new wave is as effective in promoting the continued transfer of energy to the internal wave as the

original wave. The phase of the new wave, Θ_4 , can be inferred from the measured surface elevation. The fact that little distortion in the profile was observed during the interaction of experiment 5 indicates near equality of the phase of the new wave Θ_4 with that of the wave it is replacing Θ_1 . This is not true of experiments 4 and 6. A noticeable distortion in the profile of Plate V-1 indicates that the phase of one of the new surface waves is not the same as that of the initial, higher frequency surface wave. Hence it is not as efficient in maintaining the growth of the internal wave. It is suggested that this explains the discrepancy between the theoretical and observed growth of the internal wave of Figure V-5.

From the above results, it appears that the presence of a large internal wave can trigger significant exchange of energy among surface waves without, necessarily, having to greatly affect the internal wave itself. Hence, an internal wave may act as a catalyst in promoting energy transfer among surface waves at a lower order, formally, than surface gravity wave-wave interactions.

Comparing the interaction coefficients derived for the two layer and linear stratifications, one finds that in the limit

$$\chi_3 D \gg 1 ,$$

$$\frac{I_{N=\text{const.}}}{I_{2\,\text{layer}}} \sim \frac{\exp \chi_3 d}{2(\chi_3 D)^2} \ll 1 .$$

This result is also valid for progressive wave interactions and is impor- for oceanographic applications. One sees how the presence of a near surface thermocline enhances the surface-surface-internal wave interaction over that which one might expect with a constant N model. Kenyon's (1968) estimate for a deep ocean with a constant Brunt frequency predicts small energy transfer for this mechanism compared to other possibilities. A density profile typical of a tropical or seasonal thermocline should permit much larger energy transfer between two surface and one internal gravity wave.

As mentioned in Phillips (1966), the maximum transfer of energy from a beam of surface waves would be to internal waves propagting at right angles to the directionality in the surface wave field. This is due to the form of the interaction integral(4b.11):

$$\int_{-D}^{0} f_3^*(z)\left[\sum_i\sum_j \eta_i - \mathcal{L}\{\tilde{w}\}\right]dz \sim -\int_{-D}^{0} f_3^*(z)\mathcal{L}\{\tilde{w}\}\,dz \propto \int f_3^*(z)\, e^{-|\underline{\chi}_1-\underline{\chi}_2|z}\,dz ,$$

where $f_3^*(z)$ is the conjugate vertical eigen function for an internal wave, and $exp\{-|\underline{\chi}_1-\underline{\chi}_2|z\}$ arises from the surface wave forcing at the free surface. The surface wavenumbers $\underline{\chi}_1$ and $\underline{\chi}_2$ have been assumed to be nearly equal in magnitude. Kenyon (1968) found a similar maximum transfer at right angles to the surface wave field using a Lagrangian formulation. As yet, no observations of oceanic surface and internal waves have been sufficient to prove or disprove the surface wave generation mechanism for internal waves.

EXPERIMENTAL APPENDIX

The calibration of the A/0 refractometer was done by accurately weighing a fixed volume of fluid, standardizing against distilled water, then measuring the index of refraction of a sample. Figure A-1 is a plot of eleven calibration points, a second order polynomial fit to the data, and a published calibration curve. If $\sigma = (\rho-1)\times 10^3 = A + B\Delta n + C(\Delta n)^2$ then the fit to the data points gives A=0.3, B=.399, C=5.35x10^{-5}. The published curve is $\sigma = .410\,\Delta n$.

A static calibration of two surface wave probes is shown in Figure A-2. An additional stage of amplification removing the DC offset was necessary. Shown in Plate A-1 is the wavegauge. More detailed description can be found in McGoldrick (1969).

The wave tank, wave maker and filling apparatus are shown in Plate A-2.

Table 1 contains a summary of the parameter values used in the experiments.

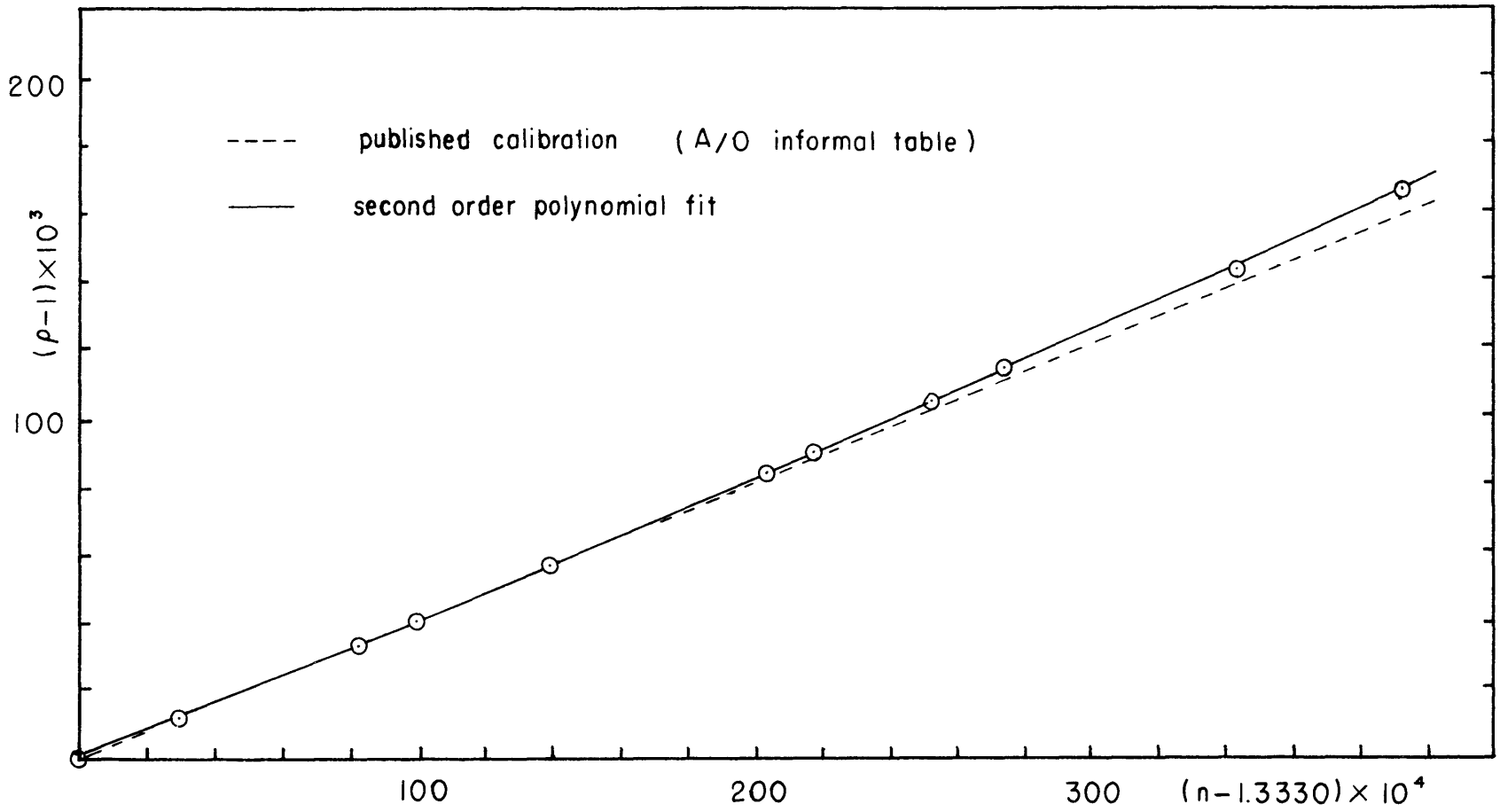

Figure A-1 Calibration of A/0 refractometer

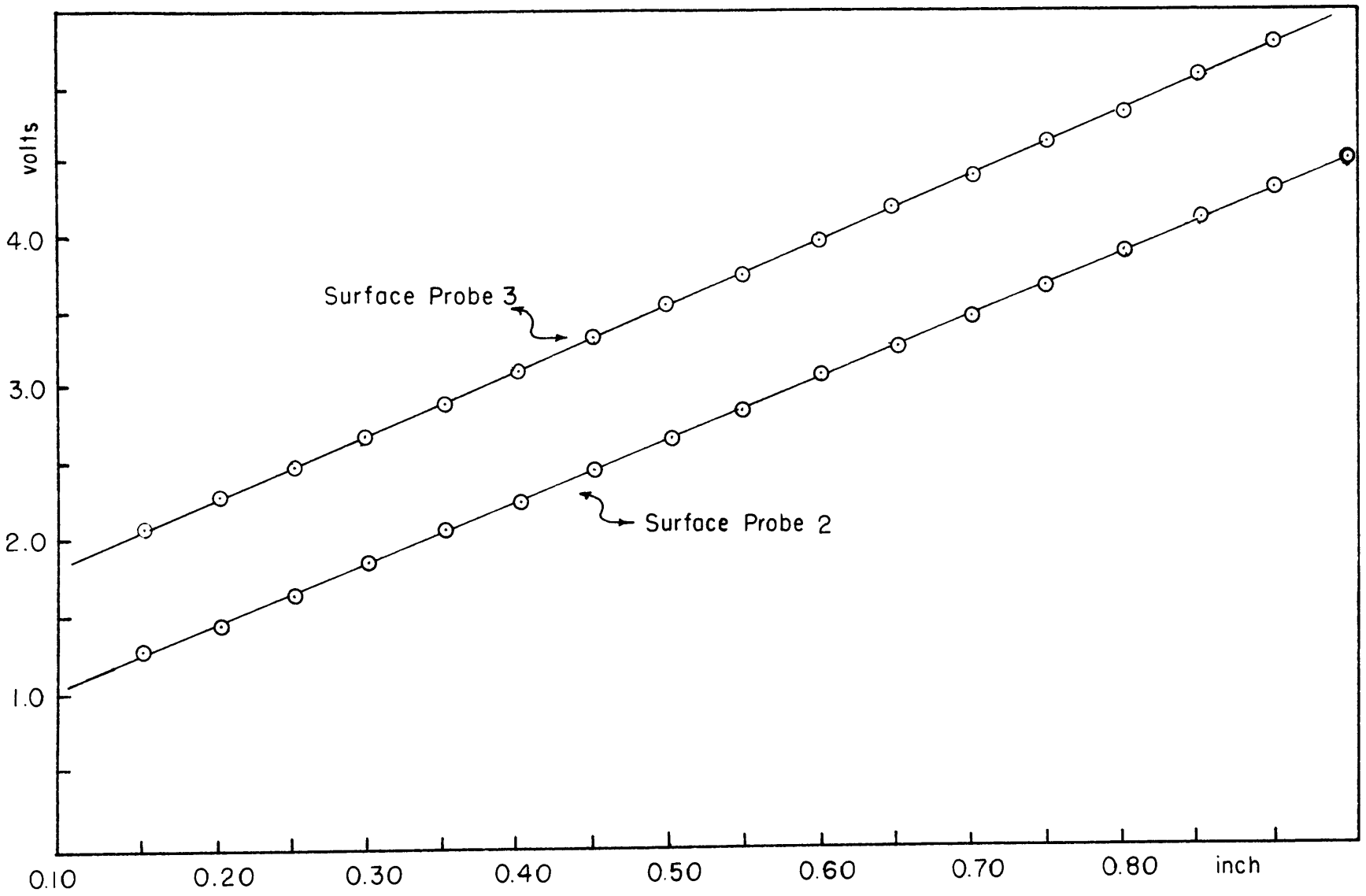

Figure A-2 Static calibration of surface probes

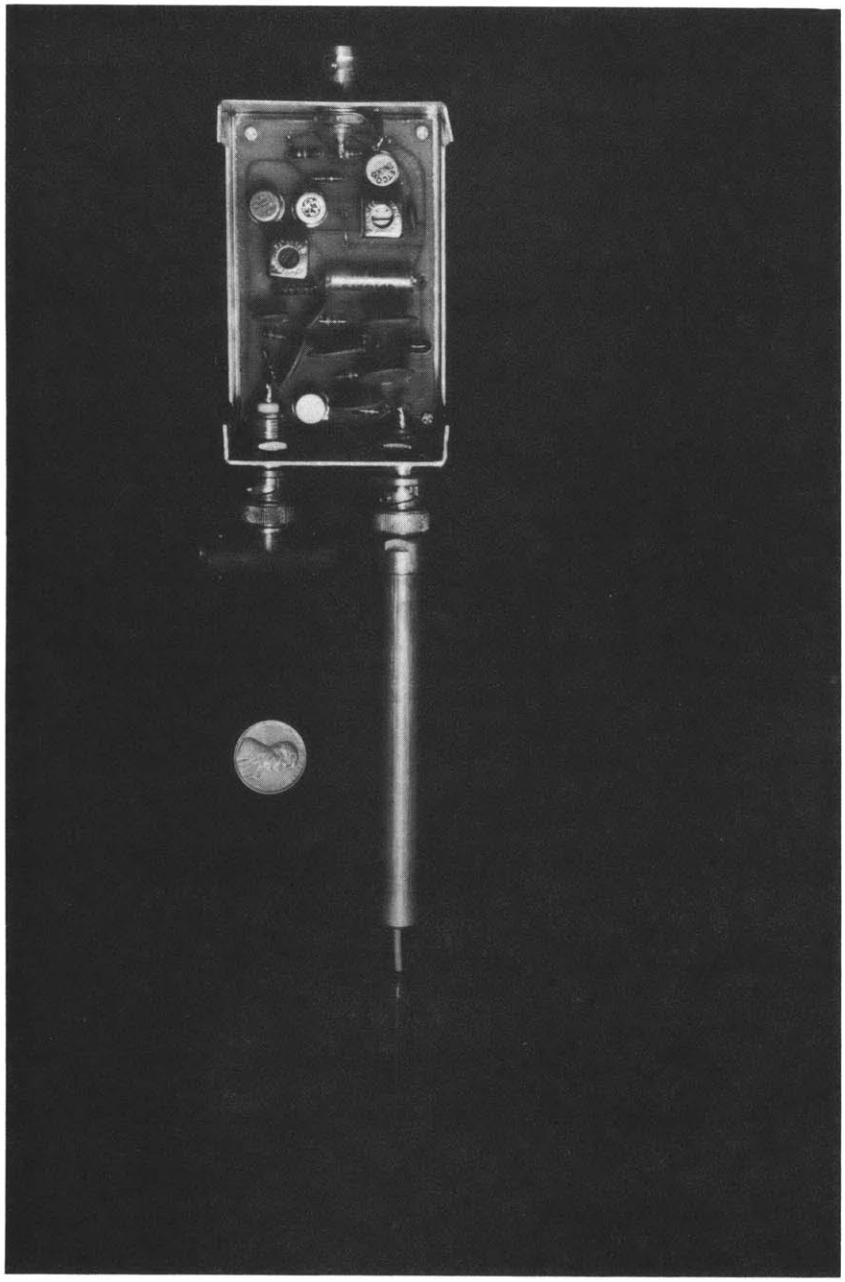

Plate A-1 Surface Probe

Plate A-2 Wave Tank

TABLE 1

$\lambda' = \left(\frac{\sigma_3}{2\pi}\right)^{-1}\lambda$		σ_{01}(rad/sec) / σ_{02}	σ_{03} / σ_{03}(linear theory)	a_1(mm)	a_2(mm)	a_3(mm)	n	ρ_{max}	N_{max}(rad/sec)
.071	Exp. 4c	18.20 17.72	.484 .492	3.77	2.68	5.5	1	1.049	4.9
.040	Exp. 5	18.91 17.88	1.034 1.015	2.79	2.36	5.75	2	1.077	4.76
.086	Exp. 6	18.20 17.71	.493 .488	3.75	2.68	4.75	1	1.116	$\overline{N}$ 1.10

THEORETICAL APPENDIX

I. Viscous boundary layer dissipation

A. Two layer model

If $\underline{q}_i \cos(\sigma t+\theta)$ is the interior velocity of the standing internal wave, then the total velocity field satisfying a no-slip boundary condition is

$$\underline{q}_T = \underline{q}_i \left[\cos(\sigma t+\theta) - e^{-\zeta} \cos(\sigma t+\theta-\zeta) \right],$$

where $$\zeta = \gamma \sqrt{\frac{\sigma}{2\nu}}$$

and γ is the normal to the rigid surface. The total dissipation per unit area in the boundary layer is $\mu \int_0^\infty \sqrt{\frac{2\nu}{\sigma}} \left(\frac{\partial \underline{q}_T}{\partial \gamma} \cdot \frac{\partial \underline{q}_T}{\partial \gamma} \right) d\zeta$. Since little horizontal motion due to the internal wave was observed at the free surface, it will be considered a no-slip surface. For the internal wave field represented by (4b.25) the total dissipation due to side wall boundary layers in one wave period is

$$D_1 = \sigma R_e^{-1/2} Q E,$$

where

$$R_e^{-1} = \frac{\nu \chi^2}{\sigma},$$

$$Q = \frac{2}{\chi W} + \frac{2}{\chi L} + \frac{\rho^U \left[1+2\frac{d}{L}\right] \sinh^{-2}\chi d + \rho^L \left[1+2\frac{D-d}{L}\right] \sinh^{-2}\chi(D-d)}{\rho^U \coth\chi d + \rho^L \coth\chi(D-d)}$$

where W is the width of the tank,

and $$E = \left(\frac{1}{2}\right)\left(\frac{2\pi}{\sigma}\right)\left(\frac{L}{2}\right)(W)\, g\, \Delta\rho \sinh^2 \chi d$$

is the total energy of the internal wave.

Dissipation at the diffuse interface has been calculated using a model in which the Brunt-Väisälä frequency is everywhere zero except in a thin layer of thickness ℓ in which it is a constant and much larger than the wave frequency σ. It is possible to match up horizontal and vertical velocities of the top and bottom layers. In this region

$$\left\{\frac{\partial^2}{\partial t^2}\left(\frac{\partial^2}{\partial x^2}+\frac{\partial^2}{\partial z^2}\right)+N^2\frac{\partial^2}{\partial x^2}\right\}w \sim \left\{\frac{\partial^2}{\partial t^2}\frac{\partial^2}{\partial z^2}+N^2\frac{\partial^2}{\partial x^2}\right\}w = 0.$$

The dissipation per unit area in this region is

$$\int_{-d+\ell/2}^{-d+\ell/2} \mu\left(\frac{\partial u}{\partial z}\right)^2 dz \sim \mu\left(\frac{\partial u}{\partial z}\right)^2 \ell, \quad \text{for } N = \text{const.}$$

the total dissipation in this layer is

$$D_2 = 2\sigma\, Re^{-1}\left(\frac{N}{\sigma}\right)^2 E.$$

If

$$\frac{dE}{dt} = -(D_1+D_2) = -2\lambda E,$$

then the dissipation constant λ is given by

$$\lambda = \frac{\sigma}{2} Re^{-1/2}\left\{Q + 2\left(\frac{N^2}{\sigma^2}\right)Re^{-1/2}\right\}.$$

For the two layer experiments,

$$Re^{-1/2} \doteq 2\times10^{-3}, \qquad \frac{2\frac{N^2}{\sigma^2}Re^{-1/2}}{Q} \doteq 0.1$$

B. Linear Stratification

Using the result of McEwan (1971), the dissipation parameter for side wall boundary layers may be written (with notational change and correction of a glaring typographical error)

$$\lambda = \frac{\sigma}{2} Re^{-1/2}\left(\frac{\sigma}{N}\right)^2 \frac{1}{xV}\left[\left(\frac{L}{D}\right)^2(DL+2WL)+\left(\frac{L}{D}\right)(DL+2WD)\right],$$

where $Re^{-1} = \frac{\nu \chi^2}{\sigma}$, W = width , V = volume $(L \cdot D \cdot W)$.

When evaluated for the parameters of experiment 6 , this gives $\lambda' = \frac{2\pi}{\sigma}\lambda = 0.05$ wheras the measured decay rate with both motors off was 0.086 . For the purposes of the calculators in chapter V, the measured value was used.

II. A note on the method of tuning

If one of the surface waves is a normal mode (i.e. $\sigma_1 = \sigma_{01}$) but the other is not then

$$\eta_1 = a_1 \cos \chi_1 x \cos(\sigma_1 t + \theta_1)$$
$$\eta_2 \neq a_2 \cos \chi_2 x \cos(\sigma_2 t + \theta_2)$$

but $$\eta_2 = \sum_n a_2^n \cos \chi_2^n x \cos(\sigma_2 t + \theta_2^n)$$

where $$\chi_2^n = \frac{n\pi}{L} \quad , \quad n = 1, 2, \ldots$$

Nonlinear products such as $\eta_1 \eta_2$ contribute to the forcing of the internal wave. If we are interested in an internal wave with wave number $\chi_3 = \chi_1 - \chi_2$ then $\frac{2}{L}\int_0^L \eta_1 \eta_2 \cos \chi_3 x \, dx$

gives the contribution of this product term to the forcing of that internal wave. But

$$\frac{2}{L}\int_0^L \eta_1\eta_2\cos\chi_3 x\,dx = a_1a_2\cos\left(\sigma_1+r\sigma_2 t+\theta_1+r\theta_2\right)\delta\left(\chi_2-\chi_2^n\right)$$

where

$$r=\pm 1\ ,\quad \delta\left(\chi_2-\chi_2^n\right)=\begin{cases}1\ , & \chi_2=\chi_2^n\\ 0\ , & \chi_2\neq\chi_2^n\end{cases}$$

Hence one of the surface waves can be a "forced" wave yet still contribute to the interaction.

The method of tuning is described in chapter II. It was convenient in the laboratory to just change slightly the frequency of one of the surface waves and observe the growth of the internal wave. The main disadvantage of this method is that one cannot measure a_2 without an elaborate calibration experiment. For frequencies σ_2 near σ_{o2}, however,

$$\eta_2 \sim a_2\cos\chi_2 x\cos\left(\sigma_2 t+\theta_2\right)$$

III. Nonlinear product terms

The nonlinear product term η_2 for the continuous stratification was evaluated for the case in which two surface waves were present. This term was the same as the product term in the two layer model, N_1. This should not come as a surprise as both terms came from the free surface boundary conditions. This suggests that the general case of a smoothly varying $\rho_o(z)$ could have been used for a linear stratification as well as a diffuse

two layer one. The form for N_1 is

$$N_1 = \frac{1}{4} \sum_{i \le j}^{3} \sum_{r,o} \frac{a_i a_j \sigma_i \sigma_j}{\chi_i \chi_j} \left\{ \right\} \cos(\chi_i + o\chi_j) \sin(\overline{\sigma_i + r\sigma_j} t + \theta_i + r\theta_j)$$

$$\left\{ \right\} = -r\sigma_j f_i'' f_j - \sigma_i f_i f_j'' - \chi_i \chi_j f_i f_j (r \cdot o \sigma_j + o \sigma_i) +$$

$$- r \frac{(\sigma_i + r\sigma_j)}{g} (r\sigma_j f_i' f_j + \sigma_i f_i f_j') + (\sigma_i + r\sigma_j)(f_i' f_j' - o \chi_i \chi_j f_i f_j)$$

If subscripts 1 and 2 refer to surface waves, then $N_1 (i=1, j=2)$ reduces to $N_1^{1,2} = \frac{1}{g} a_1 a_2 \sigma_1 \sigma_2 \sigma_3$

The back interaction terms can be found by permuting the indices i, j. Since the nonlinear products already appear in the equation governing the surface waves, averaged equations for the slowly varying amplitudes a_1, a_2 and phases θ_1, θ_2 can be found directly. Simmons (1969) obtained general inviscid solutions for phases θ_j and amplitudes a_j in the form of elliptic functions. In order to model the experiment described here, however, one would also have to include viscosity and paddle forcing.

BIOGRAPHICAL SKETCH

The author, Terrence M. Joyce, was born in Highland Falls, New York, on 13 May 1946. Most of his early years were spent in Griffith, Indiana where he attended elementary and secondary schools. In 1964, he enrolled at Rose Polytechnic Institute, Terre Haute, Indiana. While there he played football and studied physics. In March of 1968, he graduated Summa Cum Laude with a B.S. in physics. One month later he was married to Karen M. Schreiner, a graduate in Speech and Hearing Therapy at Purdue University.

While still an undergraduate, the author attended a Summer School in Environmental Science, sponsored by the University of Miami and directed by Kuldip Chopra. It was there that interest in oceanography was aroused. In June of 1968, the author entered M.I.T.-Woods Hole Oceanographic Institute Joint Program. Funding during the first three years in graduate school was under an NDEA Title IV fellowship. The final year was spent as a research assistant under Robert C. Beardsley at M.I.T.

While at M.I.T., the author was commissioned a 2nd Lieut. in the U. S. Army Reserve, and a daughter, Jennifer Anne (one year), was born into the world.

REFERENCES

Ball, F. K., 1964: Energy transfer between external and internal gravity waves. J. Fluid Mech., 19, 465.

Beardsley, R. C., 1969: An experimental study of inertial waves in a closed cone. M.I.T. Geophysical Fluid Dynamics Laboratory report, GFD/69-1.

Benjamin, T. B. and J. E. Feir, 1967: The disintegration of wave trains on deep water. J. Fluid Mech., 27, 417.

Bogoluibov, N. N. and Y. A. Mitropolsky, 1961: Asymptotic methods in the theory of non-linear oscillations. Hindustan Publishing Company (translated from Russian).

Cacchione, D. A., 1970: Experimental study of internal gravity waves over a slope. Ph.D. Thesis, M.I.T.-W.H.O.I., Joint Program in Oceanography.

Craik, A. D. D., 1971: Non-linear resonant instability in boundary layers. J. Fluid Mech., 50, 393.

Davis, R. E. and A. Acrivos, 1967: The stability of oscillatory internal waves. J. Fluid Mech., 30, 723.

Hasselmann, K. A., 1966: Feynman diagrams and interaction rules of wave-wave scattering processes. Rev. Geophys., 4, 1.

Hasselmann, K. A., 1967: A criterion for non-linear wave stability. J. Fluid Mech., 30, 737.

Kenyon, K., 1968: Wave-wave interactions of surface and internal waves. J. Marine Research, 26, 3, 208.

Kim, Y. K. and T. J. Hanratty, 1971: Weak quadratic interactions of two dimensional waves. J. Fluid Mech., 50, 107.

Kraus, W., 1966: Interne Wellen, Gebrüder Borntraeger, Berlin-Nikolassee.

Lamb, H.: Hydrodynamics, 1945, (6th edit.), Dover Publications, New York.

Longuet-Higgins, M. S., 1962: Resonant interactions between two trains of gravity waves. J. Fluid Mech., 12, 321.

Longuet-Higgins, M. S. and N. D. Smith, 1966: An experiment on third order resonant wave interactions. J. Fluid Mech., 25, 417.

Martin, S., W. F. Simmons and C. Wunsch, 1969: Resonant internal wave interactions. Nature, 224, 1014.

Martin, S., W. F. Simmons and C. Wunsch, 1972: The excitation of resonant triads by single internal waves. J. Fluid Mech., (in press).

McEwan, A. D., 1971: Degeneration of resonantly-excited standing internal gravity waves. J. Fluid Mech., 50, 431.

McGoldrick, L. F., 1965: Resonant interactions among capillary-gravity waves. J. Fluid Mech., 21, 305.

McGoldrick, L. F., O. M. Phillips, N. Huang and T. Hodgson, 1966: Measurements on resonant wave interactions. J. Fluid Mech., 25, 437.

McGoldrick, L. F., 1969: A system for the generation and measurement of capillary-gravity waves. Tech. Rep. no. 3, Department of the Geophysical Sciences, Univ. of Chicago.

McGoldrick, L. F., 1970: An experiment on second-order capillary-gravity resonant wave interactions. J. Fluid Mech., 40, 251.

Phillips, O. M., 1960: On the dynamics of unsteady gravity waves of finite amplitude. J. Fluid Mech., 9, 193.

Phillips, O. M., 1966: Dynamics of the upper ocean. Cambridge University Press.

Phillips, O. M., 1967: Theoretical and experimental studies of gravity wave interactions. Proc. Roy. Soc. A., 299, 104.

Simmons, W. F., 1969: A variational method for weak resonant wave interactions. Proc. Roy. Soc. A., 309, 551.

Thorpe, S. E., 1966A: On wave interactions in a stratified fluid. J. Fluid Mech., 24, 737.

Thorpe, S. E., 1966B: Internal gravity waves. Ph.D. Thesis, University of Cambridge.

Yih, C., 1965: Dynamics of nonhomogeneous fluids, New York, MacMillan.